

Tidal interactions and
principle of corresponding states:
from micro to macro cosmos.
A century after van der Waals' Nobel Prize

R. Caimmi*

February 21, 2022

Abstract

The current paper was aimed to honor the first centennial of Johannes Diderik van der Waals (VDW) awarding Nobel Prize in Physics. VDW theory of ordinary fluids is reviewed in the first part of the paper, where special effort is devoted to the equation of state and the law of corresponding states. In addition, a few mathematical features involving properties of cubic equations are discussed, for appreciating the intrinsic beauty of VDW theory. A theory of astrophysical fluids is shortly reviewed in the second part of the paper, grounding on the tensor virial theorem for subsystems, and an equation of state is formulated with convenient choices of reduced variables. Additional effort is devoted to selected density profiles, namely a simple guidance case and two cases of astrophysical interest. Given the analogy between macrogas reduced isoenergetics and VDW reduced isothermals, a phase transition (gas-stars) is assumed to take place in astrophysical fluids, similarly to a phase transition (vapour-liquid) observed in ordinary fluids. In this framework, the location of gas clouds, stellar

**Physics and Astronomy Department, Padua University, Vicolo Osservatorio 3/2, 35122 Padova, Italy. Affiliated up to September 30th 2014. Current status: Studioso Senior. Current position: in retirement due to age limits.*
email: roberto.caimmi@unipd.it fax: 39-049-8278212

systems, galaxies, cluster of galaxies, on the plane scanned by reduced variables, is tentatively assigned. A brief discussion shows how VDW' two great discoveries, namely a gas equation of state where tidal interactions between molecules are taken into account and the law of corresponding states, related to microcosmos, find a counterpart with regard to macrocosmos. In conclusion, after more than a century since the awarding of the Nobel Prize in Physics, VDW' ideas are still valid and helpful today for a full understanding of the universe.

keywords - gas: ideal, real - gas: equation of state - galaxies: evolution - dark matter: haloes.

1 Introduction

More than one century ago (1910), the Nobel Prize in Physics was awarded to Johannes Diderik van der Waals (hereafter quoted as VDW). In his doctoral thesis (1873) the ideal gas equation of state was generalized for embracing both the gaseous and the liquid state, where these two states of aggregation not only merge into each other in a continuous manner, but are in fact of the same nature. With respect to ideal gases, the volume of the molecules and the intermolecular tidal forces were taken into account.

VDW equation of state was later reformulated in terms of reduced (dimensionless) variables (1880), which allows the description of all substances in terms of a single equation. In other words, the state of any substance, defined by the values of reduced volume, reduced pressure, and reduced temperature, is independent of the nature of the substance. This result is known as the law of corresponding states.

VDW equation of state, in dimensional and reduced form, served as a guide during experiments which ultimately led to hydrogen (1898) and helium (1908) liquefaction. The Cryogenic Laboratory at Leiden had developed under the influence of VDW's theories. For further details on VDW's biography an interested reader is addressed to specific textbooks (e.g., Nobel Lectures 1967).

The current paper was intended to be written in honor of the first centennial of VDW awarding Nobel Prize in Physics¹. Ideal and VDW equation of state, both in dimensional and reduced form, are reviewed, and a number of features are analysed in detail, in Section 2. Counterparts to ideal and VDW equations of state for astrophysical fluids, or macrogases, are briefly summarized and compared with the classical formulation in Section 3. The

¹ It is a revised and improved version of a previous, unpublished paper available on the arxiv site (arXiv:1210.3688v1).

discussion and the conclusion are drawn in Section 4 and 5, respectively.

2 Equation of state of ordinary fluids

Let ordinary fluids be conceived as fluids which can be investigated in laboratory. The simplest description is provided by the theory of ideal gas, where the following restrictive assumptions are made: (i) particles are identical spheres; (ii) the number of particles is extremely large; (iii) the motion of particles is random; (iv) collisions between particles or with the wall of the box are perfectly elastic; (v) interactions between particles or with the wall of the box are negligible.

Ideal gas equation of state may be written under the form (e.g., Landau and Lifchitz, 1967, Chap. IV, §42, hereafter quoted as LL67):

$$pV = NkT \quad ; \quad (1)$$

where p is pressure, V volume, T temperature, N particle number, and k Boltzmann constant.

In getting a better description of ordinary fluids, the above assumption (v) is relaxed and tidal interactions between particles, due to charge distribution, are taken into consideration. VDW' generalization of the equation of state of ideal gases, Eq. (1), reads (van der Waals, 1873):

$$\left(p + A \frac{N^2}{V^2} \right) (V - NB) = NkT \quad ; \quad (2)$$

where A and B are constants which depend on particle nature.

More specifically, the presence of an attractive interaction between particles reduces both force and frequency of particle-wall collisions: the net effect is a reduction of pressure, proportional to square numerical density, expressed as $A(N/V)^2$. On the other hand, the whole volume of the box, V , is not accessible to particles, in that they are represented as identical spheres: the free volume within the box is $V - NB$, where NB is the covolume. In particular, $T = 0$ implies $V = NB$, hence the covolume per particle, B , may be conceived as the volume filled by a single sphere in the limit of zero absolute temperature.

Let $2r_0$ be the interparticle distance when the interaction energy is null (positive values being related to lower distances, implying repulsion, and negative values to larger distances, implying attraction). Accordingly, r_0 may be conceived as the effective radius of a single sphere, which implies an effective volume, $V_0 = (4\pi/3)r_0^3$. It can be seen B exceeds V_0 by a factor of

4. For further details, an interested reader is addressed to specific textbooks (e.g., LL67, Chap. VII, §§72-74).

The features of both ideal and VDW isothermal i.e. constant-temperature curves, or isothermals, were described in an earlier investigation (Caimmi 2010, hereafter quoted as C10), to be conceived as the parent paper. A comparison between VDW and empirical isothermals with equal temperature shows satisfactory agreement only in presence of a sole phase (gas or liquid) i.e. for sufficiently low or large volumes and/or sufficiently high temperatures. If, on the other hand, two phases coexist, the pressure of saturated vapour maintains constant as volume changes, yielding a horizontal real isothermal. Real isothermals are less and less extended for increasing temperature, until a single point is attained, $P_c \equiv (V_c, p_c, T_c)$, which is defined as critical point. The special VDW isothermal where the critical point lies, is defined as critical isothermal.

Parameters appearing in VDW equation of state, Eq. (2), may be expressed in terms of coordinates of critical point, as:

$$V_c = 3NB \quad ; \quad (3)$$

$$T_c = \frac{8}{27} \frac{A}{Bk} \quad ; \quad (4)$$

$$p_c = \frac{1}{27} \frac{A}{B^2} \quad ; \quad (5)$$

$$Z_c = \frac{p_c V_c}{NkT_c} = \frac{3}{8} \quad ; \quad (6)$$

where, in general, the compressibility factor:

$$Z = \frac{pV}{NkT} \quad ; \quad (7)$$

defines the degree of departure from the behaviour of ideal gases, for which $Z = 1$, according to Eq. (1). For further details, an interested reader is addressed to specific textbooks (e.g., Rostagni, 1957, Chap. XII, §20; LL67, Chap. VIII, §85); and to the parent paper (C10).

Ideal and VDW isothermals with equal temperature are plotted in Fig. 1 for different values of T/T_c with respect to the parent paper (C10). Special regions and loci on the Clapeyron plane, (OVp) , are represented in Fig. 2 for VDW isothermals. The comparison between real and VDW isothermals with equal temperature, $T/T_c = 20/23$, is shown in Fig. 3.

For simplifying both notation and calculations, the (dimensionless) reduced variables are defined as (e.g., LL67, Chap. VIII, §85):

$$\Psi = \frac{V}{V_c} \quad ; \quad \phi = \frac{p}{p_c} \quad ; \quad \mathcal{T} = \frac{T}{T_c} \quad ; \quad (8)$$

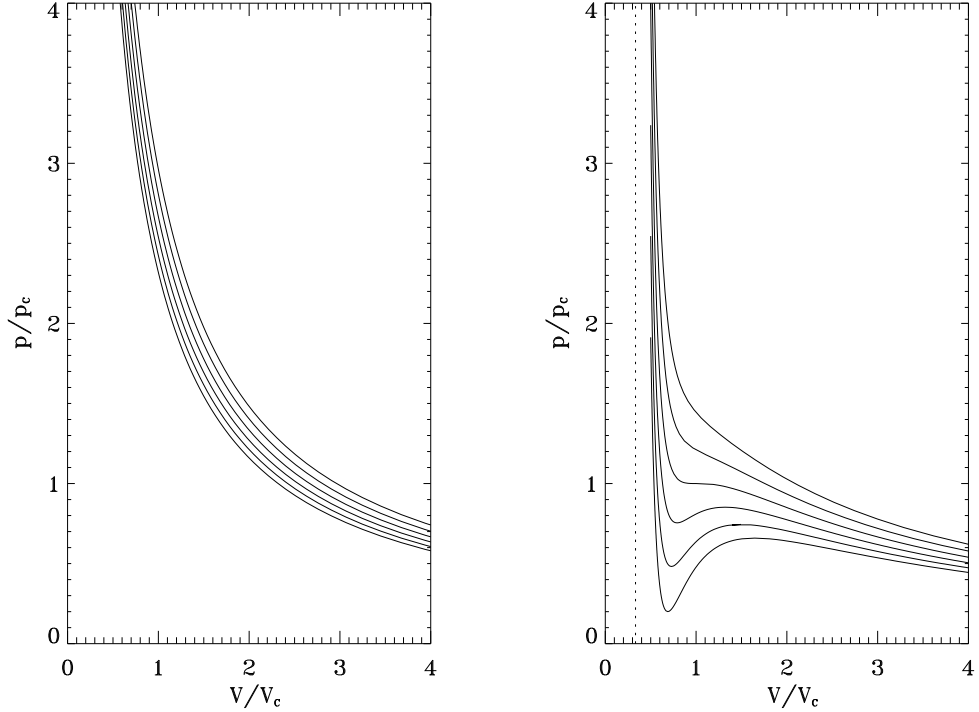


Figure 1: Ideal (left panel) and VDW (right panel) isothermals with equal temperature (from bottom to top), $T/T_c = 20/23, 20/22, 20/21, 20/20, 20/19, 20/18$. No extremum point exists above the critical isothermal, $T/T_c = 1$.

where the coordinates of the critical point are expressed by Eqs. (3), (4), and (5). Accordingly, ideal gas equation of state, Eq. (1), and VDW equation of state, Eq. (2), reduce to:

$$p\mathcal{V} = \frac{8}{3}\mathcal{T} ; \quad (9)$$

$$\left(p + \frac{3}{\mathcal{V}^2}\right) \left(\mathcal{V} - \frac{1}{3}\right) = \frac{8}{3}\mathcal{T} ; \quad \mathcal{V} > \frac{1}{3} ; \quad (10)$$

respectively. Additional features related to VDW isothermals are outlined in Appendix A. The intersections between real and VDW isothermals of equal temperature are analysed and discussed in Appendix B. The limit of absolute zero temperature is considered in Appendix C.

The locus of intersections between VDW and real isothermals of equal temperature is represented in Fig. 2 as a dashed trifid curve, where the left,

the right, and the middle branch correspond to \mathcal{V}_A , \mathcal{V}_E , and \mathcal{V}_C , shown in Fig. 3, respectively. The branching point coincides with the critical point. The locus of VDW isothermal extremum points is represented in Fig. 2 as a dotted bifid curve starting from the critical point, where the left and the right branch corresponds to minimum and maximum points, respectively.

A fluid state can be represented in reduced variables as $(\mathcal{V}, \mathcal{p}, \mathcal{T})$, where one variable may be expressed as a function of the remaining two, by use of ideal gas reduced equation of state, Eq. (9), or VDW reduced equation of state, Eq. (10). The formulation in terms of reduced variables, Eq. (8), makes related equation of state universal i.e. it holds for any fluid. Similarly, the Lane-Emden equation expressed in polytropic (dimensionless) variables describes the whole class of polytropic gas spheres, with assigned polytropic index, in hydrostatic equilibrium (e.g., Chandrasekhar 1939, Chap. IV, §4).

The coordinates of intersection points between real and VDW isothermals of equal temperature and extremum points of VDW isothermals, for selected temperatures below the critical value, are listed in Table 1 where special effort has been devoted to the lower neighbourhood of the critical point. More specifically, the following dimensionless parameters have been evaluated vs temperature, \mathcal{T} : lower volume limit, \mathcal{V}_A , where liquid and vapour phase coexist; extremum point (minimum) volume, \mathcal{V}_B ; intermediate volume, \mathcal{V}_C , where liquid and vapour phase coexist, for which pressure equals its counterpart related to corresponding lower and upper volume limit; extremum point (maximum) volume, \mathcal{V}_D ; upper volume limit, \mathcal{V}_E , where liquid and vapour phase coexist; extremum point (minimum) pressure, \mathcal{p}_B ; pressure, $\mathcal{p}_A = \mathcal{p}_C = \mathcal{p}_E$, related to horizontal real isothermal; extremum point (maximum) pressure, \mathcal{p}_D .

Tidal interactions between particles appear in Eq. (2) via parameters A and B . To gain more insight, the product on the left-hand side therein can be developed grouping the terms in A , B , AB , and combining with Eqs. (3), (5), (7), and (8). The result is:

$$pV \left(1 + \frac{9\mathcal{V} - \mathcal{p}\mathcal{V}^2 - 3}{3\mathcal{p}\mathcal{V}^3} \right) = NkT \quad ; \quad (11)$$

$$Z = \frac{pV}{NkT} = \left(1 + \frac{9\mathcal{V} - \mathcal{p}\mathcal{V}^2 - 3}{3\mathcal{p}\mathcal{V}^3} \right)^{-1} \quad ; \quad (12)$$

where the effect of tidal interactions relates to the second term within brackets. More specifically, two additional parameters i.e. critical volume and critical pressure, appear in the above mentioned term. Accordingly, VDW equation of state exhibits three variables, V , p , T , and two parameters, V_c , p_c , related to the effects of tidal interactions between particles.

Table 1: Values of dimensionless parameters, \mathcal{T} , \mathcal{V}_A , \mathcal{V}_B , \mathcal{V}_C , \mathcal{V}_D , \mathcal{V}_E , ϕ_B , ϕ_C , ϕ_D , within the range, $0.85 \leq \mathcal{T} \leq 0.99$, using a step, $\Delta \mathcal{T} = 0.01$. Additional values are computed near the critical point, to increase the resolution. All values equal unity on the critical point. Index captions: A, C, E - intersections between VDW and real isothermals of equal temperature; B - extremum point of minimum; D - extremum point of maximum. Extremum points are related to VDW isothermals, while their real counterparts are flat in presence of both liquid and vapour phase. To save aesthetics, 01 on head columns stands for unity and 9.99̄ on bottom left stands for 9.999.

$10 \mathcal{T}$	$10 \mathcal{V}_A$	$10 \mathcal{V}_B$	01 \mathcal{V}_C	01 \mathcal{V}_D	01 \mathcal{V}_E	$10 \phi_B$	$10 \phi_C$	$10 \phi_D$
8.50	5.5336	6.7168	1.1453	1.7209	3.1276	0.4963	5.0449	6.2055
8.60	5.6195	6.8003	1.1337	1.6821	2.9545	1.2750	5.3125	6.4005
8.70	5.7116	6.8883	1.1225	1.6436	2.7909	2.0346	5.5887	6.6011
8.80	5.8106	6.9814	1.1116	1.6052	2.6360	2.7752	5.8736	6.8076
8.90	5.9176	7.0804	1.1009	1.5669	2.4889	3.4965	6.1674	7.0205
9.00	6.0340	7.1860	1.0905	1.5285	2.3488	4.1984	6.4700	7.2401
9.10	6.1615	7.2994	1.0804	1.4900	2.2151	4.8807	6.7816	7.4669
9.20	6.3022	7.4221	1.0706	1.4511	2.0869	5.5430	7.1021	7.7014
9.30	6.4593	7.5561	1.0610	1.4117	1.9634	6.1849	7.4318	7.9443
9.40	6.6369	7.7040	1.0516	1.3715	1.8438	6.8058	7.7707	8.1963
9.50	6.8412	7.8697	1.0425	1.3300	1.7271	7.4049	8.1188	8.4584
9.60	7.0819	8.0593	1.0336	1.2867	1.6118	7.9811	8.4762	8.7319
9.70	7.3756	8.2830	1.0249	1.2404	1.4960	8.5328	8.8429	9.0185
9.80	7.7554	8.5611	1.0164	1.1892	1.3761	9.0576	9.2191	9.3209
9.90	8.3091	8.9461	1.0081	1.1278	1.2430	9.5510	9.6048	9.6437
9.95	8.7471	9.2353	1.0040	1.0876	1.1618	9.7830	9.8012	9.8157
9.98	9.1727	9.5049	1.0016	1.0540	1.0972	9.9158	9.9202	9.9240
9.99	9.4018	9.6456	1.0008	1.0377	1.0670	9.9585	9.9600	9.9614
9.99̄	9.8035	9.8856	1.0001	1.0117	1.0204	9.9960	9.9960	9.9960

In terms of reduced variables, Eq. (11) via Eq. (6) reads:

$$\not{p}\mathcal{V} \left(1 + \frac{9\mathcal{V} - \not{p}\mathcal{V}^2 - 3}{3\not{p}\mathcal{V}^3} \right) = \frac{8}{3}T \quad ; \quad (13)$$

where the term within brackets tends to zero as $\mathcal{V} \rightarrow 1/3$ i.e. volume reduces to covolume, which implies null temperature, as expected.

3 Equation of state of astrophysical fluids

3.1 General considerations

Let macrogases be defined as astrophysical fluids confined by gravitation. Let two-component system be taken into consideration. For assigned density profiles, the virial theorem can be formulated for each subsystem, where the potential energy is the sum of the self potential energy of the component under consideration, and the tidal energy induced by the other one. Accordingly the virial theorem for subsystems reads:

$$2(E_u)_{\text{kin}} + (E_{uv})_{\text{vir}} = 0 \quad ; \quad (u, v) = (i, j), (j, i) \quad ; \quad (14a)$$

$$(E_{uv})_{\text{vir}} = (E_u)_{\text{sel}} + (E_{uv})_{\text{tid}} \quad ; \quad (14b)$$

where i and j denote inner and outer subsystem², respectively, E_{kin} is kinetic energy, E_{sel} , E_{tid} , and E_{vir} are self, tidal, and virial potential energy, respectively. For further details, an interested reader is addressed to the parent paper (C10).

Astrophysical fluids differ from ordinary fluids on two main respects, namely (i) the latter are collisional while the former could be collisionless, which implies rectilinear and curvilinear trajectories, respectively, and (ii) macrogases cannot be bounded by rigid walls, which implies evaporation. The assumption of closed systems needs nonzero pressure on related boundaries, where evaporating macroparticles are forced to be reflexed as in rigid walls.

Observables in ordinary fluids (e.g., volume, pressure, temperature) within cylindrical boxes may be changed acting on a movable circular wall or piston, by adding or subtracting mechanical energy or work. Conceptually, nothing changes if the box and the piston are thought to be spherical and the surface of the piston to be variable³.

²For sake of simplicity, configurations with intersecting boundaries shall not be considered in the current investigation.

³A simpler example relates to ordinary fluids inside conical boxes with a changing-surface piston moving along the axis of the cone.

By analogy, astrophysical fluids must necessarily be conceived as two-component fluids, where one subsystem, G, is the macrogas under consideration, and the other one, P, acts as a piston for changing the observables. Energy can be added to or subtracted from P subsystem (and then to G subsystem via tidal interaction) by changing the mass, M_P , and/or the volume, V_P , and/or the density profile, ρ_P , and determining the virial equilibrium configuration via the virial theorem for subsystems. Let related observables be defined as macrovolume, V_U , macropressure, p_U , and macrotemperature, T_U , $U = G, P$.

Macrovolume is merely the volume filled by macrogas. Macropressure has necessarily dimensions of force per unit area or energy per unit volume, regardless of (dimensionless) shape factors and profile factors. If macroparticles are conceived as mass points, macrotemperature may be defined as in ordinary fluids:

$$T_U = \frac{1}{3} \frac{2(E_U)_{\text{kin}}}{N_U k} = \frac{1}{3} \frac{\bar{m}_U (\sigma_U)^2}{k} ; \quad U = G, P ; \quad (15)$$

where N is total number of macroparticles, $\bar{m} = M/N$ mean macroparticle mass, σ rms velocity, and k Boltzmann constant. For typical stellar systems, $\bar{m} = 1m_\odot$, $\sigma = 144$ km/s, macrotemperature is $T = 10^6$ K. The large value of macrotemperature with respect to temperature in ordinary fluids arises from the large value of mean macroparticle mass with respect to mean particle mass in ordinary fluids.

Strictly speaking, Eq. (15) holds for collisional fluids, where the stress tensor is isotropic. For collisionless fluids, the stress tensor is in general anisotropic. In any case, it is diagonal in the reference frame where the coordinate axes coincide with the principal axes of inertia. Accordingly, the macrotemperature tensor may be defined as:

$$(T_U)_{pp} = \frac{1}{3} \frac{2[(E_U)_{pp}]_{\text{kin}}}{N_U k} = \frac{1}{3} \frac{\bar{m}_U [(\sigma_U)_{pp}]^2}{k} ; \quad p = 1, 2, 3 ; \quad (16)$$

$$[(\sigma_U)_{11}]^2 + [(\sigma_U)_{22}]^2 + [(\sigma_U)_{33}]^2 = (\sigma_U)^2 ; \quad U = G, P ; \quad (17)$$

$$(T_U)_{11} + (T_U)_{22} + (T_U)_{33} = T_U ; \quad U = G, P ; \quad (18)$$

in the following, attention shall be restricted to macrotemperature i.e. the trace of macrotemperature tensor.

For assigned subsystems, $(U, V) = (G, P), (P, G)$, the virial theorem reads:

$$-(E_U)_{\text{sel}} - (E_{UV})_{\text{tid}} = -(E_{UV})_{\text{vir}} = 2(E_U)_{\text{kin}} ; \quad (19)$$

according to Eq. (14). For further details, an interested reader is addressed to earlier investigations (Limber 1959; Brosche et al. 1983; Caimmi et al. 1984; Caimmi and Secco 1992).

The combination of Eqs. (15) and (19) yields:

$$-\frac{1}{3} \frac{(E_U)_{\text{sel}}}{V_U} V_U \left[1 + \frac{(E_{UV})_{\text{tid}}}{(E_U)_{\text{sel}}} \right] = N_U k T_U ; \quad (20)$$

in terms of macrotemperature. The following definition of macropressure:

$$p_U = -\frac{1}{3} \frac{(E_U)_{\text{sel}}}{V_U} ; \quad (21)$$

translates the virial theorem for subsystems into an equation of state, as:

$$p_U V_U \left[1 + \frac{(E_{UV})_{\text{tid}}}{(E_U)_{\text{sel}}} \right] = N_U k T_U ; \quad (22)$$

with regard to (U, V) macrogases, (U, V) = (G, P), (P, G). Accordingly, the ratio:

$$Z_U = \frac{p_U V_U}{N_U k T_U} = \left[1 + \frac{(E_{UV})_{\text{tid}}}{(E_U)_{\text{sel}}} \right]^{-1} ; \quad (23)$$

may be conceived as macrogas compressibility factor. In this view, Eqs. (22) and (23) are macrogas counterparts of Eqs. (11) and (12), respectively, which hold for VDW gas.

In the limit of an infinitely extended V subsystem, $V_V \rightarrow +\infty$, $(E_{UV})_{\text{tid}} \rightarrow 0$, Eq. (22) has the same formal expression as the ideal gas equation of state, Eq. (1), which, in turn, results from the VDW equation of state, Eq. (2), in absence of tidal action between molecules.

Strictly speaking, covolume, $N_U B_U$, should be taken into consideration, which should imply $V_U > N_U B_U$ instead of $V_U > 0$. In any case, $N_U B_U \ll V_U$, for astrophysical fluids, assuming either $B_G = V_\odot$, where V_\odot is the solar volume, or $B_U = (4\pi/3)[(R_U)_g]^3/N_U$, where $(R_U)_g = 2GM_U/c^2$ (c velocity of light in baryonic matter vacuum) is the gravitational radius (e.g., Landau and Lifchitz, 1966, Chap. IX, §97) of macrogas under consideration. For this reason, covolume shall be neglected in the following.

From this point on, attention shall be restricted to the special case of homeoidally striated density profiles with similar and similarly placed boundaries, where coordinate axes coincide with principal axes of inertia.

3.2 Homeoidally striated density profiles with similar and similarly placed boundaries

For homeoidally striated density profiles with similar and similarly placed boundaries, where coordinate axes coincide with principal axes of inertia,

self potential energy and tidal potential energy take the explicit expression (e.g., C10):

$$(E_U)_{\text{sel}} = -\frac{G(M_U)^2}{a_U} \frac{\Xi_U(\nu_U)_{\text{sel}}}{[(\nu_U)_{\text{mas}}]^2} \Sigma ; \quad U = G, P ; \quad (24)$$

$$(E_{UV})_{\text{tid}} = -\frac{G(M_U)^2}{a_U} \frac{\Xi_U(\nu_{UV})_{\text{tid}}}{[(\nu_U)_{\text{mas}}]^2} \Sigma ; \quad (U, V) = (G, P), (P, G) ; \quad (25)$$

where G is constant of gravitation, M mass, $a = a_1$ truncation radius along the major semiaxis, $\Xi = \Xi_1$ dimensionless truncation radius along the major semiaxis, ν_{mas} and ν_{sel} are profile factors i.e. depending only on the density profile, ν_{tid} is a profile factor which, in addition, depends on the mass ratio, $m = M_P/M_G$, and on the homodirection axis ratio, $y = a_P/a_G = (a_P)_r/(a_G)_r$, $r = 1, 2, 3$, and Σ is a shape factor i.e. depending only on the boundary, where $\Sigma = 2$ in the special case of spherical symmetry (e.g., Caimmi and Secco 1992; Caimmi 1993, 1995).

The substitution of Eqs. (24) and (25) into (20) after little algebra yields:

$$\frac{1}{3} \frac{G(M_U)^2}{a_U} F_{UV} = N_U k T_U ; \quad (U, V) = (G, P), (P, G) ; \quad (26a)$$

$$F_{UV} = \frac{\Xi_U(\nu_U)_{\text{sel}}}{[(\nu_U)_{\text{mas}}]^2} \left[1 + \frac{(\nu_{UV})_{\text{tid}}}{(\nu_U)_{\text{sel}}} \right] \Sigma ; \quad (26b)$$

where tidal effects from V subsystem relate to the profile factor, $(\nu_{UV})_{\text{tid}}$.

In addition, Eqs. (21), (22), and (23), take the explicit form:

$$p_U = \frac{1}{4\pi} \frac{G(M_U)^2}{(a_U)^4 \epsilon_{21} \epsilon_{31}} \frac{\Xi_U(\nu_U)_{\text{sel}}}{[(\nu_U)_{\text{mas}}]^2} \Sigma ; \quad U = G, P ; \quad (27)$$

$$p_U V_U \left[1 + \frac{(\nu_{UV})_{\text{tid}}}{(\nu_U)_{\text{sel}}} \right] = N_U k T_U ; \quad (U, V) = (G, P), (P, G) ; \quad (28)$$

$$Z_U = \frac{p_U V_U}{N_U k T_U} = \left[1 + \frac{(\nu_{UV})_{\text{tid}}}{(\nu_U)_{\text{sel}}} \right]^{-1} ; \quad (U, V) = (G, P), (P, G) ; \quad (29)$$

where $\epsilon_{pq} = a_p/a_q$ are homosurface axis ratios. For further details, an interested reader is addressed to the parent paper (C10), keeping in mind that macropressure therein has a different definition where neither profile factors nor shape factors are involved.

It is worth remembering Eqs. (28) and (29) exhibit a similar formal expression with respect to VDW gases, Eqs. (11) and (12), respectively, where the effects of tidal interactions relate to the second term within brackets. More specifically, two additional parameters i.e. mass ratio and homodirection axis ratio appear in the above mentioned term. Accordingly, macrogas

equation of state exhibits three variables, V_U , p_U , T_U , and two parameters, m , y , related to the effects of tidal interactions between subsystems.

For an arbitrary macroisothermal curve, $T_U = \text{const}$, or macroisothermal, the macrogas equation of state, Eq. (28), may be expressed as:

$$\frac{p_U V_U}{M_U} \left[1 + \frac{(\nu_{UV})_{\text{tid}}}{(\nu_U)_{\text{sel}}} \right] = \frac{kT_U}{\bar{m}_U} ; \quad (U, V) = (G, P), (P, G) ; \quad (30)$$

where $0 < V_U < +\infty$ and $(\nu_{UV})_{\text{tid}}/(\nu_U)_{\text{sel}} \geq 0$ in the case under consideration of homeoidally striated density profiles with similar and similarly placed boundaries, as shown below. For homogeneous spherical configurations, $\Xi = 1$, $\nu_{\text{mas}} = \Xi^3 = 1$, $\nu_{\text{sel}} = 3\Xi^5/10 = 3/10$, $\epsilon_{pq} = 1$, $\Sigma = 2$, and Eq. (27) reduces to:

$$(p_U)_{\text{hsp}} = \frac{1}{4\pi} \frac{3G(M_U)^2}{5(a_U)^4} ; \quad (31)$$

where the index, hsp, means homogeneous sphere. Related self potential energy, via Eq. (21), is:

$$[(E_U)_{\text{sel}}]_{\text{hsp}} = -\frac{3}{5} \frac{G(M_U)^2}{a_U} ; \quad (32)$$

which may be considered as a limiting value for the following reasons.

Gravitational potential energy of a matter distribution (in absolute value) may be conceived as a binding energy which, *ipso facto*, is increasing for increasing concentration at fixed total mass and major semiaxis. Accordingly, both inhomogeneous and aspherical configurations increase the binding energy provided density profiles with positive slope are excluded as unphysical. In this view, homogeneous spherical configurations are related to a minimum binding energy, $-[(E_U)_{\text{sel}}]_{\text{hsp}} \leq -(E_U)_{\text{sel}}$.

On the other hand, the tidal action exerted from the external homeoid of the outer subsystem on the inner one is null owing to Newton's theorem, which implies $(E_{ij})_{\text{tid}}/(E_i)_{\text{sel}} = (\nu_{ij})_{\text{tid}}/(\nu_i)_{\text{sel}} > 0$. In addition, the tidal action exerted from the inner subsystem on the outer one implies $(E_{ji})_{\text{tid}}/(E_j)_{\text{sel}} = (\nu_{ji})_{\text{tid}}/(\nu_j)_{\text{sel}} > 0$. This is why the presence of a second subsystem enhances binding energy with respect to a single subsystem. In conclusion, $(E_{UV})_{\text{tid}}/(E_U)_{\text{sel}} = (\nu_{UV})_{\text{tid}}/(\nu_U)_{\text{sel}} > 0$, $(U, V) = (G, P), (P, G)$.

According to the above considerations, the left-hand side of Eq. (28) via (20)-(22) satisfies the following condition:

$$\begin{aligned} p_U V_U \left[1 + \frac{(\nu_{UV})_{\text{tid}}}{(\nu_U)_{\text{sel}}} \right] &= -\frac{1}{3} [(E_U)_{\text{sel}} + (E_{UV})_{\text{tid}}] \\ &= \frac{1}{3} \frac{G(M_U)^2}{a_U} \frac{\Xi_U (\nu_U)_{\text{sel}}}{[(\nu_U)_{\text{mas}}]^2} \left[1 + \frac{(\nu_{UV})_{\text{tid}}}{(\nu_U)_{\text{sel}}} \right] \Sigma > \frac{1}{3} \frac{3G(M_U)^2}{5 a_U} ; \end{aligned} \quad (33)$$

or:

$$\frac{\Xi_U(\nu_U)_{\text{sel}}}{[(\nu_U)_{\text{mas}}]^2} \left[1 + \frac{(\nu_{UV})_{\text{tid}}}{(\nu_U)_{\text{sel}}} \right] \Sigma > \frac{3}{5} ; \quad (34)$$

which depends on the density profiles (including shape) and, in addition, on the homodirection axis ratio, y , and the mass ratio, m , via $(\nu_{UV})_{\text{tid}}$.

Let (V_U, p_U) be an assigned state on a selected macroisothermal, $T_U = \text{const.}$ An increasing macrovolume, V_U , or major semiaxis, a_U , at constant mass, M_U , implies a decreasing left-hand side of Eq. (28), via Eq. (27), which may be compensated by increasing concentration and/or asphericity via Eq. (34), with due account taken of a changing tidal interaction due to the factor, $[1 + (\nu_{UV})_{\text{tid}}/(\nu_U)_{\text{sel}}]$, appearing in Eq. (28), until an infinite macrovolume is attained. In particular, $[\Xi\nu_{\text{sel}}/(\nu_{\text{mas}})^2]\Sigma = 3/(5-n)$ for polytropic spheres of polytropic index equal to n ($0 \leq n \leq 5$), $\Sigma = \pi$ for flattened oblate spheroids ($\epsilon_{21} = 1, \epsilon_{31} \rightarrow 0$), and $\Sigma \rightarrow +\infty$ for elongated prolate spheroids ($\epsilon_{21} = \epsilon_{31} \rightarrow 0$).

A decreasing macrovolume, V_U , or major semiaxis, a_U , at constant mass, M_U , implies an increasing left-hand side of Eq. (28), via Eq. (27), which may be compensated by decreasing concentration and/or asphericity via Eq. (34), with due account taken of a changing tidal interaction via the factor, $[1 + (\nu_{UV})_{\text{tid}}/(\nu_U)_{\text{sel}}]$, appearing in Eq. (28), until a minimum macrovolume is attained, which makes the ending point of the macroisothermal. In fact, lower macrovolumes would imply density profiles with positive slope, unless the assumption of mass conservation is released. By increasing mass, a macroisothermal can be continued until null macrovolume (or volume equal to covolume) is asymptotically attained.

Accordingly, astrophysical fluids lying on macroisothermals must be conceived as open systems i.e. variable macroparticle number, contrary to ordinary fluids, which can be conceived as closed systems i.e. constant particle number. Then a more germane formulation of macrogas equation of state, Eq. (30), reads:

$$\frac{p_U}{\bar{\rho}_U} \left[1 + \frac{(\nu_{UV})_{\text{tid}}}{(\nu_U)_{\text{sel}}} \right] = \frac{kT_U}{\bar{m}_U} ; \quad (U, V) = (G, P), (P, G) ; \quad (35)$$

where mean density, $\bar{\rho} = M/V$, appears instead of total mass, M .

Dividing both sides of Eq. (28) where $(U, V) = (P, G)$, by their counterparts where $(U, V) = (G, P)$, yields:

$$Y_P Y_V \frac{1 + (\nu_{PG})_{\text{tid}}/(\nu_P)_{\text{sel}}}{1 + (\nu_{GP})_{\text{tid}}/(\nu_G)_{\text{sel}}} = \frac{N_P}{N_G} Y_T ; \quad (36)$$

in terms of the dimensionless variables:

$$Y_P = \frac{p_P}{p_G} ; \quad Y_V = \frac{V_P}{V_G} ; \quad Y_T = \frac{T_P}{T_G} ; \quad (37)$$

or, using Eqs. (15) and (27):

$$Y_P = \frac{m^2 \Xi_P (\nu_P)_{\text{sel}} \left[\frac{(\nu_G)_{\text{mas}}}{(\nu_P)_{\text{mas}}} \right]^2}{y^4 \Xi_G (\nu_G)_{\text{sel}}} ; \quad Y_V = y^3 ; \quad Y_T = \frac{N_G}{N_P} \phi ; \quad (38)$$

$$m = \frac{M_P}{M_G} ; \quad y = \frac{a_P}{a_G} ; \quad \phi = \frac{(E_P)_{\text{kin}}}{(E_G)_{\text{kin}}} = \frac{(E_{PG})_{\text{vir}}}{(E_{GP})_{\text{vir}}} ; \quad (39)$$

where the mass ratio, m , has not to be confused with the mean macroparticle mass, \bar{m} . The combination of Eqs. (15) and (37)-(39) yields:

$$T_P = \frac{\bar{m}_P}{\bar{m}_G} \frac{\phi}{m} T_G ; \quad (40)$$

where $\bar{m}_P = \bar{m}_G$ without loss of generality, provided P macrogas is considered only for the tidal potential induced on G macrogas.

Owing to Eqs. (38) and (39), Eq. (36) by use of (26b) takes the explicit form:

$$\frac{m^2 F_{PG}}{y F_{GP}} = \phi ; \quad (41)$$

in terms of the dimensionless variables (C10):

$$X_P = m^2 ; \quad X_V = \frac{1}{y} ; \quad X_T = \phi ; \quad (42)$$

where the dimensionless factors, F , depend on the density profiles and, in addition, on the variables, m , y , via the profile factors, ν_{tid} .

In the case under consideration of homeoidally striated, similar and similarly placed ellipsoids, the dependence on the shape implies the same factor, Σ , for both F_{PG} and F_{GP} , which disappears in the ratio, F_{PG}/F_{GP} . Accordingly, Eq. (41) may be conceived as shape independent.

The additional restriction of coinciding scaled density profiles, $f_U = \rho_U/\rho_U^\dagger$, $\rho_U^\dagger = \rho_U(r_U^\dagger)$, r_U^\dagger selected scaling radius along a fixed direction, $U = G,P$; coinciding scaled truncation radii, $\Xi_U = R_U/r_U^\dagger$, R_U truncation radius along the same direction, $U = G,P$; and coinciding homodirection axes, $y = 1$, makes Eq. (41) reduce to:

$$m = \phi ; \quad y = 1 ; \quad (43)$$

for a formal demonstration, an interested reader is addressed to the parent paper (C10).

Due to appearance of parameters from both G and P macrogases, Eq. (36) or equivalently Eq. (41) may be conceived as a macrogas reduced equation of state, depending only on dimensionless parameters. More specifically, macrogas reduced equation of state, Eq. (41), depends on three dimensionless variables, namely mass ratio, m , homodirection axis ratio, y , and kinetic energy ratio, ϕ , which is the counterpart of VDW reduced equation, Eq. (13), for VDW gases.

For assigned macrogases, the locus, $\phi = \text{const}$, on the dimensionless plane, $(Oy^{-1}m^2)$, may be conceived as a fractional isoenergetic curve, or fractional isoenergetic, in the sense that kinetic energy ratio, ϕ , instead of macrotemperature ratio, Y_T , maintains constant. It can be seen the latter alternative implies a subdomain where configurations have no physical meaning. For further details, an interested reader is addressed to Appendix D.

A generic point, (X_V, X_p) , on a fractional isoenergetic, X_T , is connected to an infinity of configurations where homodirection axis ratio, y , mass ratio, m , kinetic energy ratio, ϕ , remain unchanged. Accordingly, macrogas equations of state, Eqs. (26), are “entangled”: for fixed $a_U, M_U, (E_U)_{\text{kin}} = (3/2)N_U kT_U$, related counterparts $a_V, M_V, (E_V)_{\text{kin}} = (3/2)N_V kT_V$, are inferred via y, m, ϕ , by use of Eq. (39). Keeping in mind P subsystem is conceived as a piston for changing the state of the other one, attention shall mainly be restricted to G subsystem.

With regard to a generic curve on $(OX_V X_p)$ plane, and a generic subdomain, $X_{V_1} \leq X_V \leq X_{V_2}$, related area below the curve reads:

$$\mathcal{S}_{12} = \int_{X_{V_1}}^{X_{V_2}} X_p dX_V = \int_{y_1^{-1}}^{y_2^{-1}} m^2 d\frac{1}{y} = \int_{y_2}^{y_1} \frac{m^2}{y^2} dy ; \quad (44)$$

where, in particular, mass, M_G , and radius, a_G , can be left unchanged while M_P and a_P vary via Eqs. (39) and (42). Accordingly, Eq. (44) translates into:

$$\mathcal{S}_{12} \frac{GM_G^2}{a_G} = \int_{a_{P_2}}^{a_{P_1}} \frac{GM_P^2}{a_P^2} da_P ; \quad (45)$$

which may be conceived as the work performed on G macrogas via P macrogas to leave M_G and a_G unchanged passing from (M_{P_1}, a_{P_1}) to (M_{P_2}, a_{P_2}) .

A similar result holds for a generic curve on the $(OX_V^{-1} X_p^{-1})$ plane, where the counterpart of Eq. (45) exhibiting indexes, G and P, reversed, may be conceived as the work performed on P macrogas via G macrogas to leave M_P and a_P unchanged passing from (M_{G_1}, a_{G_1}) to (M_{G_2}, a_{G_2}) .

Macrogas equation of state, Eq. (28) via Eqs. (15) and (26) exhibits three variables, $a_G, M_G, (E_G)_{\text{kin}}$, and two parameters, m, y , which are fixed by the point selected on the fractional isoenergetic, where a third parameter, ϕ ,

remains unchanged. If, in addition, attention is restricted to isoenergetics, $(E_G)_{\text{kin}} = (3/2)N_G k T_G = \text{const}$, where mass conservation, $M_G = \text{const}$, $N_G = \text{const}$, takes place, then $T_G = \text{const}$, and the remaining variable, a_G , can be determined via Eq. (26).

It is worth emphasizing fractional isoenergetics, $X_T = \text{const}$, and fractional macroisothermals, $Y_T = (N_G/N_P)\phi = (\bar{m}_P/\bar{m}_G)(\phi/m) = \text{const}$ via Eq. (40), are equivalent provided mass conservation takes place in both macrogases. The same holds for isoenergetics, $(E_U)_{\text{kin}} = (3/2)N_U k T_U = \text{const}$ via Eq. (15), and macroisothermals, $T_U = \text{const}$.

For assigned shape, density profiles, and truncation radii, isoenergetics or macroisothermals can be determined along the following steps.

- (i) Start from a generic configuration among (m, y) .
- (ii) For assigned $\phi = X_T$, via Eq. (41) plot related fractional isoenergetic on $(OX_V X_P)$ plane.
- (iii) For assigned mass, M_G , and kinetic energy, $(E_G)_{\text{kin}} = N_G k T_G$, via Eq. (26) determine major semiaxis, a_G and via Eq. (39) determine M_P , a_P , $(E_P)_{\text{kin}} = N_P k T_P$.
- (iv) Return to (iii) and change m, y , along the fractional isoenergetic leaving $M_G, N_G k T_G$, unchanged.
- (v) Using Eq. (27), determine $p_G, V_G; p_P, V_P$; and plot related isoenergetics on $(OV_G p_G); (OV_P p_P)$; plane, respectively.
- (vi) Return to (ii) and repeat the procedure until a family of fractional isoenergetics is plotted on $(OX_V X_P)$ plane, and a family of isoenergetics is plotted on $(OV_G p_G)$ and $(OV_P p_P)$ plane for different $N_G k T_G$ and $N_P k T_P$, respectively.

Accordingly, a selected isoenergetic on the plane, $(OV_G p_G)$, Eq. (28), corresponds to a fractional isoenergetic on the dimensionless plane, $(OX_V X_P)$, Eq. (41), and vice versa, conformly to Eqs. (37)-(40).

The procedure outlined above defines a special way of making macroisothermal changes of state, $(V_G, p_G, T_G) \rightarrow (V_G + \Delta V_G, p_G + \Delta p_G, T_G)$, and in this sense it is not restrictive. With regard to ordinary fluids, it is equivalent to vary mechanical and thermal energy by assigned amounts making isothermal changes of state, $(V, p, T) \rightarrow (V + \Delta V, p + \Delta p, T)$.

The definition of dimensionless variables, Y_V, Y_P, Y_T , expressed by Eq. (37), aims to a closer analogy between ordinary and astrophysical fluids with respect to the parent paper (C10) where attention was restricted to X_V, X_P, X_T ,

expressed by Eq. (42), and fractional isoenergetics were conceived as macroisothermals.

Fractional isoenergetics were derived in the parent paper (C10) for a wide amount of cases, with regard to different kind of macrogases, namely UU, HH, and HN/NH. More specifically, UU is a simple guidance case where no critical point occurs; conversely, HH and HN/NH are cases of astrophysical interest where critical points take place. Accordingly, isoenergetics can be inferred from the above mentioned fractional isoenergetics.

Critical fractional isoenergetics, hosting a critical point i.e. a horizontal inflexion point, take place in macrogases for sufficiently steep density profiles: fractional isoenergetics on one side exhibit two extremum points (maximum and minimum), while fractional isoenergetics on the other side exhibit no extremum point, similarly to reduced VDW isothermals. On the contrary, critical fractional isoenergetics are absent for sufficiently mild density profiles, where fractional isoenergetics show a nonmonotonic trend. For further details, an interested reader is addressed to the parent paper (C10) and an earlier investigation (Caimmi and Valentinuzzi 2008).

The existence of a phase transition moving along a selected fractional isoenergetic in presence of extremum points (model fractional isoenergetic), where the path is a horizontal line (transition fractional isoenergetic), must necessarily be assumed as a working hypothesis, due to the analogy between VDW isothermals and model fractional isoenergetics. Unlike VDW equation of state, Eq. (2), macrogas equation of state, Eq. (30), is not analytically integrable, which implies the procedure, used for determining a selected fractional isoenergetic, must be numerically performed.

The main steps are the following.

- (i) Calculate intersections, V_{GA} , V_{GC} , V_{GE} ; $V_{GA} < V_{GC} < V_{GE}$; between the generic horizontal line on the plane, $(OV_G p_G)$, $p_G = \text{const}$, and the curve related to theoretical macrogas equation of state, within the range, $p_{GB} < p_G < p_{GD}$, where B and D denote extremum points of minimum and maximum, respectively.
- (ii) Calculate area of regions, ABC and CDE.
- (iii) Find the special value, $p_G = p_{GC}$, which makes regions of equal area.
- (iv) Trace the transition fractional isoenergetic as a horizontal line connecting points, (V_{GA}, p_{GA}) , (V_{GC}, p_{GC}) , (V_{GE}, p_{GE}) , $p_{GA} = p_{GC} = p_{GE}$.

For further details, an interested reader is addressed to the parent paper (C10). In order to preserve the analogy with ideal and VDW gases, the

tidal potential energy has to be negligible and comparable, respectively, with regard to self potential energy, in the formulation of the virial theorem for subsystems and related equation of state concerning macrogas of interest.

For assigned density profiles allowing critical macroisothermal, Eqs. (28), (U, V) = (G, P), (36), and (41), may be translated into reduced variables, as:

$$\phi_G \Psi_G \frac{1 + (\nu_{GP})_{\text{tid}}/(\nu_G)_{\text{sel}}}{1 + [(\nu_{GP})_{\text{tid}}]_c/(\nu_G)_{\text{sel}}} = \frac{M_G}{(M_G)_c} \mathcal{T}_G ; \quad (46)$$

$$\phi_G = \frac{p_G}{(p_G)_c} ; \quad \Psi_G = \frac{V_G}{(V_G)_c} ; \quad \mathcal{T}_G = \frac{T_G}{(T_G)_c} ; \quad (47)$$

$$Y_P Y_V F_c = \frac{m}{m_c} Y_T ; \quad (48)$$

$$Y_P = \frac{Y_p}{Y_{pc}} ; \quad Y_V = \frac{Y_V}{Y_{Vc}} ; \quad Y_T = \frac{Y_T}{Y_{Tc}} ; \quad (49)$$

$$F_c = \frac{1 + (\nu_{PG})_{\text{tid}}/(\nu_P)_{\text{sel}}}{1 + [(\nu_{PG})_{\text{tid}}]_c/(\nu_P)_{\text{sel}}} \frac{1 + [(\nu_{GP})_{\text{tid}}]_c/(\nu_G)_{\text{sel}}}{1 + (\nu_{GP})_{\text{tid}}/(\nu_G)_{\text{sel}}} ; \quad (50)$$

$$\mathcal{X}_P \mathcal{X}_V F_c = \mathcal{X}_T ; \quad (51)$$

$$\mathcal{X}_P = \frac{X_P}{X_{pc}} ; \quad \mathcal{X}_V = \frac{X_V}{X_{Vc}} ; \quad \mathcal{X}_T = \frac{X_T}{X_{Tc}} ; \quad (52)$$

where the index, c, denotes critical point, and dimensionless variables, X, are defined by Eq. (42).

In the limit of an infinitely extended P subsystem, $y \rightarrow +\infty$, $(\nu_{PG})_{\text{tid}} \rightarrow 0$, $(\nu_{GP})_{\text{tid}} \rightarrow 0$, Eqs. (46) and (48) reduce to:

$$\phi_G \Psi_G = \left\{ 1 + \frac{[(\nu_{GP})_{\text{tid}}]_c}{(\nu_G)_{\text{sel}}} \right\} \frac{M_G}{(M_G)_c} \mathcal{T}_G ; \quad (53)$$

$$Y_P Y_V = \frac{1 + [(\nu_{PG})_{\text{tid}}]_c/(\nu_P)_{\text{sel}}}{1 + [(\nu_{GP})_{\text{tid}}]_c/(\nu_G)_{\text{sel}}} \frac{m}{m_c} Y_T ; \quad (54)$$

which can be related to ordinary gases filling a fixed volume. For further details, an interested reader is addressed to the parent paper (C10).

The above result, expressed by Eq. (46), may be written in parametric form using Eqs. (27) and (28), as:

$$\phi_G = \frac{\mathcal{M}_G^2}{\phi_G^4} ; \quad \Psi_G = \phi_G^3 ; \quad \mathcal{T}_G = \frac{\mathcal{M}_G}{\phi_G} \chi_c ; \quad (55)$$

$$\phi_G = \frac{a_G}{(a_G)_c} ; \quad \mathcal{M}_G = \frac{M_G}{(M_G)_c} ; \quad \chi_c = \frac{1 + (\nu_{GP})_{\text{tid}}/(\nu_G)_{\text{sel}}}{1 + [(\nu_{GP})_{\text{tid}}]_c/(\nu_G)_{\text{sel}}} ; \quad (56)$$

where ϕ_G and \mathcal{M}_G may be conceived as reduced radius and reduced mass, respectively.

Reduced macropressure and reduced macrotemperature, as functions of reduced macrovolume, read:

$$\not{p}_G = \not{M}_G^2 \not{V}_G^{-4/3} ; \quad \not{T}_G = \not{M}_G \not{V}_G^{-1/3} \chi_c ; \quad (57)$$

where the dependence on the path along a fractional isoenergetic, $\phi = \text{const}$, occurs via χ_c . The dependence of reduced macropressure, \not{p}_G , and reduced macrotemperature, \not{T}_G , on reduced macrovolume, \not{V}_G , for assigned reduced mass, \not{M}_G , and parameter, χ_c , is shown in Fig.4 where macrogas state is defined by the intersection of two selected curves together with related point on fractional isoenergetic, (m, y, ϕ) .

The dependence of reduced macrotemperature i.e. χ_c , on reduced coordinate, \not{X}_V , for fixed reduced volume and reduced mass, or reduced coordinate, \not{X}_T , is owing to density profiles and shall be determined for UU, HH, HN/NH macrogases in the following sections.

3.3 UU macrogases

UU macrogases exhibit flat density profiles, which is equivalent to polytropes of index, $n = 0$ (e.g., Chandrasekhar 1939, Chap.IV, §4; Caimmi 1986; Caimmi 2016), but implies negative distribution functions for stellar fluids (Vandervoort 1980). For this reason, UU macrogases are of little astrophysical interest and can be considered as a simple guidance case.

Fractional isoenergetics ($X_T = \text{const}$) may be explicitly expressed as (C10):

$$X_p = \frac{X_T}{X_V} [1 + \Psi(X_V, X_T)] ; \quad (58a)$$

$$\Psi(X_V, X_T) = \begin{cases} \frac{X_V^5 \Phi^2(X_V, X_T)}{2X_T} - \frac{X_V^3 \Phi(X_V, X_T)}{X_T} \sqrt{\frac{X_V^4 \Phi^2(X_V, X_T)}{4} + \frac{X_T}{X_V}} ; \\ 0 < X_V \leq 1 ; \\ \frac{\Phi^2(X_V, X_T)}{2X_V^5 X_T} - \frac{\Phi(X_V, X_T)}{X_V^2 X_T} \sqrt{\frac{\Phi^2(X_V, X_T)}{4X_V^6} + \frac{X_T}{X_V}} ; \\ 1 \leq X_V < +\infty ; \end{cases} \quad (58b)$$

$$\Phi(X_V, X_T) = \begin{cases} \frac{5}{2} \frac{1}{X_V^2} - \frac{3}{2} - X_T ; & 0 < X_V \leq 1 ; \\ 1 - \left(\frac{5}{2} X_V^2 - \frac{3}{2} \right) X_T ; & 1 \leq X_V < +\infty ; \end{cases} \quad (58c)$$

$$\lim_{X_V \rightarrow 0^+} X_p = \lim_{X_V \rightarrow 0^+} \frac{X_T}{X_V} = +\infty ; \quad \lim_{X_V \rightarrow +\infty} X_p = \lim_{X_V \rightarrow +\infty} \frac{X_T}{X_V} = 0 ; \quad (58d)$$

$$\lim_{X_T \rightarrow 0^+} X_p = 0 ; \quad \lim_{X_T \rightarrow +\infty} X_p = +\infty ; \quad (58e)$$

where X_p , X_V , X_T , are dimensionless variables defined by Eq.(42).

Plotting fractional isoenergetics, $X_p(X_V)$, for assigned X_T , on $(OX_V X_p)$ plane, shows two extremum points (minimum and maximum, respectively) but no critical point within the domain, $0 < X_T < +\infty$ (C10). On the other hand, $\phi_{\text{crit}} \approx 10$, $m_{\text{crit}} \approx 10$, for HH and HN/NH macrogases (C10). Then $\phi_{\text{norm}} = 10$ shall be arbitrarily assumed as normalization value, together with $y_{\text{norm}} = 1.186944$ implying $m_{\text{norm}} = 7.290778$ via Eqs. (58a)-(58c). The result is:

$$\begin{aligned} X_{V_n} &= \frac{1}{y_{\text{norm}}} = 0.8425 \quad ; \quad X_{p_n} = (m_{\text{norm}})^2 = 53.15545 \quad ; \\ X_{T_n} &= \phi_{\text{norm}} = 10 \quad ; \end{aligned} \quad (59)$$

and reduced variables:

$$\mathcal{X}_V = \frac{X_V}{X_{V_n}} \quad ; \quad \mathcal{X}_p = \frac{X_p}{X_{p_n}} \quad ; \quad \mathcal{X}_T = \frac{X_T}{X_{T_n}} \quad ; \quad (60)$$

shall be used in place of their counterparts related to critical values.

Fractional isoenergetics, $\mathcal{X}_p^{-1}(\mathcal{X}_V^{-1})$, are plotted in Fig. 5 for $\mathcal{X}_T^{-1} = 20/23, 20/22, 20/21, 20/20, 20/19, 20/18$, from bottom to top. The contribution from the term, $\mathcal{X}_T^{-1}/\mathcal{X}_V^{-1}$, is shown by dotted curves. More specifically, dividing both sides of Eq. (58a) by their counterparts related to $(X_{V_n}, X_{p_n}, X_{T_n})$ yields:

$$\mathcal{X}_p = \frac{\mathcal{X}_T}{\mathcal{X}_V} \frac{1 + \Psi(X_V, X_T)}{1 + \Psi(X_{V_n}, X_{T_n})} \quad ; \quad (61)$$

where the inverse of the whole product and the first factor on the right-hand side are represented in Fig. 5 as full and dotted curves, respectively. The reason for plotting \mathcal{X}_p^{-1} vs \mathcal{X}_V^{-1} instead of \mathcal{X}_p vs \mathcal{X}_V shall be clarified in dealing with HH and HN/NH macrogases.

In the case under consideration of flat density profiles, without loss of generality, scaled truncation radii can be assumed as $\Xi_U = R_U/r_U^\dagger = 1$, $U = G, P$. Accordingly, profile factors reduce to:

$$(\nu_U)_{\text{mas}} = 1 \quad ; \quad (\nu_U)_{\text{sel}} = \frac{3}{10} \quad ; \quad U = G, P \quad ; \quad (62)$$

$$(\nu_{GP})_{\text{tid}} = \begin{cases} \frac{3}{10} \frac{m}{y^3} \quad ; & 1 \leq y < +\infty \quad ; \\ \frac{3}{10} m \left(\frac{5}{2} - \frac{3}{2} y^2 \right) \quad ; & 0 < y \leq 1 \quad ; \end{cases} \quad (63)$$

$$(\nu_{PG})_{\text{tid}} = \begin{cases} \frac{3}{10} \frac{1}{m} \left(\frac{5}{2} - \frac{3}{2} \frac{1}{y^2} \right) \quad ; & 1 \leq y < +\infty \quad ; \\ \frac{3}{10} \frac{y^3}{m} \quad ; & 0 < y \leq 1 \quad ; \end{cases} \quad (64)$$

for further details, an interested reader is addressed to the parent paper (C10). The special case of coinciding volumes, $y = 1$, implies $(\nu_{\text{GP}})_{\text{tid}} = (3/10)m$; $(\nu_{\text{PG}})_{\text{tid}} = (3/10)(1/m)$; as expected.

In addition, Eqs. (26b) and (56) reduce to:

$$F_{\text{GP}} = \begin{cases} \frac{3}{10} \left(1 + \frac{m}{y^3}\right) \Sigma & ; \quad 1 \leq y < +\infty & ; \\ \frac{3}{10} \left[1 + m \left(\frac{5}{2} - \frac{3}{2}y^2\right)\right] \Sigma & ; \quad 0 < y \leq 1 & ; \end{cases} \quad (65)$$

$$F_{\text{PG}} = \begin{cases} \frac{3}{10} \left[1 + \frac{1}{m} \left(\frac{5}{2} - \frac{3}{2}\frac{1}{y^2}\right)\right] \Sigma & ; \quad 1 \leq y < +\infty & ; \\ \frac{3}{10} \left(1 + \frac{y^3}{m}\right) \Sigma & ; \quad 0 < y \leq 1 & ; \end{cases} \quad (66)$$

$$\chi_{\text{c}} = \begin{cases} \frac{1+m/y^3}{1+m_{\text{norm}}/y_{\text{norm}}^3} & ; \quad 1 \leq y < +\infty & ; \\ \frac{1+m[5/2-(3/2)y^2]}{1+m_{\text{norm}}/y_{\text{norm}}^3} & ; \quad 0 < y \leq 1 & ; \end{cases} \quad (67)$$

where $y = a_{\text{P}}/a_{\text{G}}$.

The dependence of reduced macrotemperature, \mathcal{T}_{G} , on reduced variable, \mathcal{X}_{V} , is shown in Fig. 6 for $M_{\text{G}}^{-1}\Psi_{\text{G}}^{1/3} = 1$ and $\mathcal{X}_{\text{T}}^{-1} = 20/23, 20/22, 20/21, 20/20, 20/19, 20/18$, from bottom to top. A similar trend is exhibited for critical fractional isoenergetic, $\mathcal{X}_{\text{T}}^{-1} = 1$, and $M_{\text{G}}^{-1}\Psi_{\text{G}}^{1/3} = 20/23, 20/22, 20/21, 20/20, 20/19, 20/18$, from bottom to top.

3.4 HH macrogases

HH macrogases exhibit central cusp and vanishing density at infinite distance (Hernquist 1990), and have been proved to be consistent with nonnegative distribution functions in an acceptable parameter range (Ciotti 1996).

Fractional isoenergetics on $(\text{O}\mathcal{X}_{\text{V}}\mathcal{X}_{\text{P}})$ plane show weak dependence on scaled truncation radii, $\Xi_{\text{G}}, \Xi_{\text{P}}$, including the limit, $\Xi_{\text{G}} \rightarrow +\infty, \Xi_{\text{P}} \rightarrow +\infty$, where formulation is far simpler. For this reason, attention shall be restricted to infinite scaled truncation radii, which imply infinitesimal scaling radii, r_{U}^{\dagger} , and/or infinite truncation radii, R_{U} , $\text{U} = \text{G}, \text{P}$, along an arbitrary direction. Accordingly, profile factors reduce to (C10):

$$(\nu_{\text{U}})_{\text{mas}} = 12 & ; \quad (\nu_{\text{U}})_{\text{sel}} = 12 & ; \quad \Xi_{\text{U}} \rightarrow +\infty & ; \quad \text{U} = \text{G}, \text{P} & ; \quad (68)$$

$$(\nu_{\text{GP}})_{\text{tid}} = \begin{cases} -\frac{9}{8}mw^{(\text{ext})}(z) & ; \quad 1 \leq y < +\infty & ; \\ -\frac{9}{8}\frac{m}{y}w^{(\text{int})}(z) & ; \quad 0 < y \leq 1 & ; \end{cases} \quad (69)$$

$$(\nu_{\text{PG}})_{\text{tid}} = \begin{cases} -\frac{9}{8}\frac{y}{m}w^{(\text{int})}(z) & ; \quad 1 \leq y < +\infty & ; \\ -\frac{9}{8}\frac{1}{m}w^{(\text{ext})}(z) & ; \quad 0 < y \leq 1 & ; \end{cases} \quad (70)$$

$$w^{(\text{int})}(z) = \begin{cases} -\frac{64z}{(z-1)^4} [-2(2z+1)\ln z + (z-1)(z+5)] & ; \quad z \neq 1 & ; \\ -\frac{32}{3} & ; \quad z = 1 & ; \end{cases} \quad (71)$$

Table 2: Values of scaling fractional mass, $m^\dagger = M(r_P^\dagger)/M(r_G^\dagger)$, fractional mass, m , scaling fractional radius, y^\dagger , fractional truncation radius, y , and fractional energy, ϕ , related to critical point i.e. the horizontal inflexion point on the critical fractional isoenergetic, for selected fractional scaled truncation radii, Ξ_G/Ξ_P , with regard to HH density profiles.

Ξ_G/Ξ_P	m^\dagger	m	y^\dagger	y	ϕ
0.25	20.2157	20.2157	4.2153	16.8612	18.1509
0.50	20.2148	20.2148	4.2594	08.5188	18.1500
1.00	20.2148	20.2148	4.2594	04.2594	18.1500
2.00	20.2148	20.2148	4.2641	02.1320	18.1500
4.00	20.2148	20.2148	4.2656	01.0664	18.1500

$$w^{(\text{ext})}(z) = \begin{cases} -\frac{64}{(z-1)^4} [2z(z+2) \ln z - (z-1)(5z+1)] & ; \quad z \neq 1 ; \\ -\frac{32}{3} & ; \quad z = 1 ; \end{cases} \quad (72)$$

$$z = y^\dagger = \frac{\Xi_G}{\Xi_P} y ; \quad (73)$$

where $y = a_P/a_G$. For further details, an interested reader is addressed to the parent paper (C10) and an earlier investigation (Caimmi and Valentinuzzi 2008).

Fractional isoenergetics ($\mathcal{X}_T^{-1} = \text{const}$), explicitly expressed substituting Eqs. (26b) and (68)-(73) into (41), are plotted in Fig. 7 for $\mathcal{X}_T^{-1} = 20/23, 20/22, 20/21, 20/20, 20/19, 20/18$, from bottom to top, where cases, $\Xi_G/\Xi_P = 0.25, 0.50, 1.00, 2.00, 4.00$, are superimposed. The dashed curve (including central branch) is the locus of intersections between HH fractional isoenergetics and horizontal lines yielding regions of equal area. The dotted curve is the locus of HH fractional isoenergetic extremum points. Plotting \mathcal{X}_P^{-1} vs \mathcal{X}_V^{-1} yields fractional isoenergetics similar to VDW isothermals shown in Fig. 2, where extremum points are lying below the horizontal inflexion point.

Critical points, (X_{Vc}, X_{Pc}, X_{Tc}) , can be inferred from Table 2 via Eq. (42). More specifically, values of scaling fractional mass, $m^\dagger = M(r_P^\dagger)/M(r_G^\dagger)$, fractional mass, m , fractional scaling radius, y^\dagger , fractional truncation radius, y , and fractional energy, ϕ , related to critical point i.e. the horizontal inflexion point on the critical fractional isoenergetic, are listed in Table 2 for selected fractional scaled truncation radii, Ξ_G/Ξ_P , with regard to HH density profiles.

An inspection of Table 2 discloses weak dependence of critical parameters on the ratio, Ξ_G/Ξ_P , within the range considered, leaving aside y via Eq. (73). Accordingly, critical parameters might be conceived as independent

of (infinite) scaled truncation radii to a first extent.

An inspection of Fig. 7 discloses weak dependence of fractional isoenergetics on the ratio, Ξ_G/Ξ_P , within the range considered. Accordingly, fractional isoenergetics might be conceived as independent of (infinite) scaled truncation radii to a first extent.

The dependence of reduced macrotemperature, \mathcal{T}_G , on reduced variable, \mathcal{X}_V , is shown in Fig. 8 for $M_G^{-1}V_G^{1/3} = 1$ and $\mathcal{X}_T^{-1} = 20/23, 20/22, 20/21, 20/20, 20/19, 20/18$, from bottom to top. A similar trend is exhibited for critical fractional isoenergetic, $\mathcal{X}_T^{-1} = 1$, and $M_G^{-1}V_G^{1/3} = 20/23, 20/22, 20/21, 20/20, 20/19, 20/18$, from bottom to top.

An inspection of Fig. 8 discloses weak dependence of reduced macrotemperature on the ratio, Ξ_G/Ξ_P , within the range considered. Accordingly, reduced macrotemperature might be conceived as independent of (infinite) scaled truncation radii to a first extent.

3.5 HN/NH macrogases

HN/NH macrogases exhibit central cusp and vanishing density at infinite distance, where HN means inner H density profile, related to G macrogas, and outer N density profile, related to P macrogas, $y = a_P/a_G \geq 1$, and NH means inner N and outer H, $y = a_P/a_G \leq 1$. N density profiles decline more slowly with respect to above considered H, yielding infinite mass within infinite radius (Navarro et al. 1995, 1996, 1997). HN macrogases have been proved to be consistent with nonnegative distribution functions in an acceptable parameter range (Lowenstein and White 1999) by use of a previously stated theorem (Ciotti and Pellegrini 1992).

Fractional isoenergetics on $(O\mathcal{X}_V\mathcal{X}_P)$ plane show weak dependence on scaled truncation radii, Ξ_G, Ξ_P , including the limit, $\Xi_G \rightarrow +\infty, \Xi_P \rightarrow +\infty$, where formulation is far simpler. For this reason, attention shall be restricted to infinite scaled truncation radii, which imply infinitesimal scaling radii, r_U^\dagger , and/or infinite truncation radii, R_U , $U = G, P$, along an arbitrary direction. Accordingly, profile factors reduce to (C10):

$$(\nu_U)_{\text{mas}} \rightarrow +\infty ; \quad (\nu_U)_{\text{sel}} = 36 ; \quad \Xi_U \rightarrow +\infty ; \quad (74)$$

$$U = \begin{cases} G & ; \text{ NH macrogases} \\ P & ; \text{ HN macrogases} \end{cases}$$

$$(\nu_{GP})_{\text{tid}} = \begin{cases} -\frac{9}{8}m^\dagger w_{\text{HN}}^{(\text{ext})}(z) & ; \quad 1 \leq y < +\infty ; \\ -\frac{9}{8}\frac{m^\dagger}{y^\dagger} w_{\text{NH}}^{(\text{int})}(z) & ; \quad 0 < y \leq 1 ; \end{cases} \quad (75)$$

$$(\nu_{PG})_{\text{tid}} = \begin{cases} -\frac{9}{8}\frac{y^\dagger}{m^\dagger} w_{\text{HN}}^{(\text{int})}(z) & ; \quad 1 \leq y < +\infty ; \\ -\frac{9}{8}\frac{1}{m^\dagger} w_{\text{NH}}^{(\text{ext})}(z) & ; \quad 0 < y \leq 1 ; \end{cases} \quad (76)$$

$$w_{\text{HN}}^{(\text{int})}(z) = \begin{cases} -\frac{64}{(z-1)^3}(-2z \ln z + z^2 - 1) & ; \quad z \neq 1 ; \\ -\frac{64}{3} & ; \quad z = 1 ; \end{cases} \quad (77)$$

$$w_{\text{HN}}^{(\text{ext})}(z) = \begin{cases} -\frac{64}{(z-1)^2} \left(\frac{z+1}{z-1} \ln z - 2 \right) & ; \quad z \neq 1 ; \\ -\frac{32}{3} & ; \quad z = 1 ; \end{cases} \quad (78)$$

$$w_{\text{NH}}^{(\text{int})}(z) = \begin{cases} -\frac{64z}{(z-1)^2} \left(\frac{z+1}{z-1} \ln z - 2 \right) & ; \quad z \neq 1 ; \\ -\frac{32}{3} & ; \quad z = 1 ; \end{cases} \quad (79)$$

$$w_{\text{NH}}^{(\text{ext})}(z) = \begin{cases} -\frac{64}{(z-1)^3}(z^2 - 1 - 2z \ln z) & ; \quad z \neq 1 ; \\ -\frac{64}{3} & ; \quad z = 1 ; \end{cases} \quad (80)$$

$$z = y^\dagger = \frac{\Xi_{\text{G}}}{\Xi_{\text{P}}} y ; \quad (81)$$

where $y = a_{\text{P}}/a_{\text{G}}$. For further details, an interested reader is addressed to the parent paper (C10) and an earlier investigation (Caimmi and Valentinuzzi 2008).

Fractional isoenergetics ($\mathcal{X}_{\text{T}}^{-1} = \text{const}$), explicitly expressed substituting Eqs. (26b) and (74)-(81) into (41), are plotted in Fig. 9 for $\mathcal{X}_{\text{T}}^{-1} = 20/23, 20/22, 20/21, 20/20, 20/19, 20/18$, from bottom to top, where cases, $\Xi_{\text{G}}/\Xi_{\text{P}} = 0.25, 0.50, 1.00, 2.00, 4.00$, are superimposed. The dashed curve (including central branch) is the locus of intersections between HN/NH fractional isoenergetics and horizontal lines yielding regions of equal area. The dotted curve is the locus of HN/NH fractional isoenergetic extremum points. Plotting $\mathcal{X}_{\text{P}}^{-1}$ vs $\mathcal{X}_{\text{V}}^{-1}$ yields fractional isoenergetics similar to VDW isothermals shown in Fig. 2, where extremum points are lying below the horizontal inflexion point.

Critical points, ($X_{\text{Vc}}, X_{\text{pc}}, X_{\text{Tc}}$), can be inferred from Table 3 via Eq. (42). More specifically, values of scaling fractional mass, $m^\dagger = M(r_{\text{P}}^\dagger)/M(r_{\text{G}}^\dagger)$, fractional mass, m , fractional scaling radius, y^\dagger , fractional truncation radius, y , and fractional energy, ϕ , related to critical point i.e. the horizontal inflexion point on the critical fractional isoenergetic, are listed in Table 3 for selected fractional scaled truncation radii, $\Xi_{\text{G}}/\Xi_{\text{P}}$, with regard to HN/NH density profiles.

An inspection of Table 3 discloses weak dependence of critical parameters on the ratio, $\Xi_{\text{G}}/\Xi_{\text{P}}$, within the range considered, leaving aside y via Eq. (81). Accordingly, critical parameters might be conceived as independent of (infinite) scaled truncation radii to a first extent.

An inspection of Fig. 9 discloses weak dependence of fractional isoenergetics on the ratio, $\Xi_{\text{G}}/\Xi_{\text{P}}$, within the range considered. Accordingly, fractional isoenergetics might be conceived as independent of (infinite) scaled truncation radii to a first extent.

The dependence of reduced macrotemperature, \mathcal{T}_{G} , on reduced variable,

Table 3: Values of scaling fractional mass, $m^\dagger = M(r_P^\dagger)/M(r_G^\dagger)$, fractional mass, m , scaling fractional radius, y^\dagger , fractional truncation radius, y , and fractional energy, ϕ , related to critical point i.e. the horizontal inflexion point on the critical fractional isoenergetic, for selected fractional scaled truncation radii, Ξ_G/Ξ_P , with regard to HN/NH density profiles.

Ξ_G/Ξ_P	m^\dagger	m	y^\dagger	y	ϕ
0.25	12.4148	∞	1.9785	7.9142	35.8702
0.50	12.4006	∞	2.0149	4.0298	35.8259
1.00	12.3984	∞	2.0292	2.0292	35.8190
2.00	12.3984	∞	2.0303	1.0151	35.8190
4.00	12.3984	∞	2.0303	0.5076	35.8190

\mathcal{X}_V , is shown in Fig. 10 for $\mathcal{M}_G^{-1}\mathcal{V}_G^{1/3} = 1$ and $\mathcal{X}_T^{-1} = 20/23, 20/22, 20/21, 20/20, 20/19, 20/18$, from bottom to top. A similar trend is exhibited for critical fractional isoenergetic, $\mathcal{X}_T^{-1} = 1$, and $\mathcal{M}_G^{-1}\mathcal{V}_G^{1/3} = 20/23, 20/22, 20/21, 20/20, 20/19, 20/18$, from bottom to top.

An inspection of Fig. 8 discloses weak dependence of reduced macrotemperature on the ratio, Ξ_G/Ξ_P , within the range considered. Accordingly, reduced macrotemperature might be conceived as independent of (infinite) scaled truncation radii to a first extent.

3.6 Critical curves

VDW critical isothermal and HH, HN/NH, critical fractional isoenergetic are compared in Fig. 11, where the dashed curve is the same as in Fig. 2. Accordingly, vapour and liquid phase of ordinary fluids coexist within the bell-shaped region bounded by the dashed curve. Both HH and HN/NH critical fractional isoenergetic are more extended along horizontal direction with respect to VDW critical isothermal, which implies a more flattened counterpart of the above mentioned bell-shaped region. The critical point, by definition, reads $(\mathcal{X}_{V_c}, \mathcal{X}_{P_c}, \mathcal{X}_{T_c}) \equiv (1, 1, 1)$.

4 Discussion

Tidal interactions between neighbouring bodies span across the whole admissible range of lengths in nature: from, say, atoms and molecules to galaxies and clusters of galaxies i.e. from micro to macro cosmos. Ordinary fluids

are collisional, which makes the stress tensor be isotropic and the velocity distribution obey Maxwell's law. Tidal interactions (electromagnetic in nature) therein act between colliding particles (e.g., LL67, Chap. VII, §74). Astrophysical fluids could be collisionless, which makes the stress tensor be anisotropic and the velocity distribution no longer obey Maxwell's law. Tidal interactions (gravitational in nature) therein act between single particles and the system as a whole (e.g., C10).

In both cases, an equation of state can be formulated in reduced variables: the VDW equation for ordinary fluids and an equation which depends on density profiles for astrophysical fluids. For sufficiently mild density profiles, fractional isoenergetics are characterized by the occurrence of two extremum points, similarly to isothermals where a transition from liquid to gaseous phase takes place, or vice versa. For sufficiently steep density profiles, the critical fractional isoenergetic exhibits a single horizontal inflexion point, which defines the critical point. Fractional isoenergetics below and above the critical one, show two or no extremum point, respectively, in complete analogy with VDW isothermals. In any case, the existence of an equation of state in reduced variables implies the validity of the law of corresponding states for macrogases with assigned density profiles.

For astrophysical fluids, the existence of a phase transition must necessarily be assumed as a working hypothesis by analogy with ordinary fluids. The phase transition has to be conceived between gas and stars, and the $(\mathcal{O}\mathcal{X}_V^{-1}\mathcal{X}_p^{-1})$ plane may be divided into three parts, namely

- (i) a region bounded by the critical fractional isoenergetic on the left of the critical point, and the locus of onset of phase transition on the right of the critical point, where only gas exists;
- (ii) a region bounded by the critical fractional isoenergetic on the left of the critical point, the locus of onset of phase transition on the left of the critical point, and the vertical axis, where only stars exist;
- (iii) a region bounded by the locus of onset of phase transition, and the horizontal axis, where gas and stars coexist.

The locus of onset of phase transition, not shown in Fig. 11 for reasons explained above, is similar to its counterpart related to ordinary fluids, represented by the bell-shaped curve in Fig. 11, but more extended along the horizontal direction.

In this view, elliptical and S0 galaxies lie on (ii) region unless hosting hot interstellar gas, and the same holds for globular clusters; spiral, irregular, and dwarf spheroidal galaxies lie on (iii) region, and the same holds for cluster of

galaxies; gas clouds where stars never formed lie on (i) region, and the same holds for hypothetical galaxies where stars never formed.

5 Conclusion

Van der Waals' two great discoveries, more specifically a gas equation of state where tidal interactions between molecules are taken into account and the law of corresponding states, related to microcosmos, find a counterpart with regard to macrocosmos. After more than a century since the awarding of the Nobel Prize in Physics, van der Waals' ideas are still valid and helpful to day for a full understanding of the universe.

References

- [1] Brosche, P., Caimmi, R., Secco, L.: 1983, *Astron. Astrophys.*, 125, 338.
- [2] Caimmi, R.: 1986, *Astron. Astrophys.*, 159, 147.
- [3] Caimmi, R.: 1993, *ApJ* 419, 615.
- [4] Caimmi, R.: 1995, *ApJ* 441, 533.
- [5] Caimmi, R.: 2010, *Serb. Astron. J.*, 180, 19. (C10)
- [6] Caimmi, R.: 2016, *App. Math. Sci.*, 10, 1821.
- [7] Caimmi, R., Secco, L., Brosche, P.: 1984, *Astron. Astrophys.*, 139, 411.
- [8] Caimmi, R., Secco, L.: 1992, *ApJ*, 395, 119.
- [9] Caimmi, R., Valentinuzzi, T.: 2008, *Serbian Astron. J.* 177, 15.
- [10] Chandrasekhar, S.: *An Introduction to the Study of the Stellar Structure*, University of Chicago Press (1939)
- [11] Ciotti, L.: 1996, *ApJ* 471, 68.
- [12] Ciotti, L., Pellegrini, S.: 1992, *MNRAS* 255, 561.
- [13] Hernquist, L.: 1990, *ApJ* 356, 359.
- [14] Landau, L., Lifchitz, E.: *Theorie du Champs*, Mir, Moscow (1966)

- [15] Landau, L., Lifchitz, E.: *Physique Statistique*, Mir, Moscow (1967) (LL67)
- [16] Limber, D.N.: 1959, ApJ 130, 414.
- [17] Lowenstein, M., White, R.E., III: 1999, ApJ 518, 50.
- [18] Navarro, J.F., Frenk, C.S., White, S.D.M.: 1995, MNRAS 275, 720.
- [19] Navarro, J.F., Frenk, C.S., White, S.D.M.: 1996, ApJ 462, 563.
- [20] Navarro, J.F., Frenk, C.S., White, S.D.M.: 1997, ApJ 490, 493.
- [21] Nobel Lectures, Physics 1901-1921: Elsevier Publishing Company, Amsterdam (1967)
- [22] Rostagni, A.: *Meccanica e Termodinamica*, ed. Libreria Universitaria di G. Randi, Padova (1957)
- [23] Spiegel, M.R.: *Mathematical Handbook*, Schaum's Outline Series, McGraw-Hill, Inc., New York (1968)
- [24] Vandervoort, P.O.: 1980, ApJ 240, 478.
- [25] van der Waals, J.D.: *Over de Continuïteit van den Gas-en Vloeïstoftoestand*, Doctoral Thesis, Leiden University, Leiden, 1873.

Appendix

A Additional features of VDW isothermals on the Clapeyron reduced plane

The equation of a generic VDW isothermal on the Clapeyron reduced plane, $(\mathcal{O}\mathcal{V}\mathcal{p})$, is (e.g., LL67, Chap. VIII, §85; C10):

$$\mathcal{p} = \frac{8\mathcal{T}}{3\mathcal{V} - 1} - \frac{3}{\mathcal{V}^2} ; \quad (82)$$

and the first and the second derivative with respect to \mathcal{V} read:

$$\left(\frac{\partial \mathcal{p}}{\partial \mathcal{V}}\right)_T = -\frac{24\mathcal{T}}{(3\mathcal{V} - 1)^2} + \frac{6}{\mathcal{V}^3} ; \quad (83)$$

$$\left(\frac{\partial^2 \mathcal{p}}{\partial \mathcal{V}^2}\right)_T = \frac{144\mathcal{T}}{(3\mathcal{V} - 1)^3} - \frac{18}{\mathcal{V}^4} ; \quad (84)$$

where, for assigned \mathcal{T} , the domain of the function, $\mathcal{p}(\mathcal{V})$, is $\mathcal{V} > 1/3$, $\mathcal{V} = 1/3$ is a vertical asymptote, and $\mathcal{p} = 0$ is a horizontal asymptote. In the special case of the critical point, $(\mathcal{V}, \mathcal{T}, \mathcal{p}) \equiv (1, 1, 1)$, the above mentioned derivatives are null, as expected.

The extremum points, via Eq. (83), are defined by the relation:

$$f(\mathcal{V}) = \frac{(3\mathcal{V} - 1)^2}{4\mathcal{V}^3} = \mathcal{T} ; \quad (85)$$

which is satisfied on the critical point, as expected. The function on the left-hand side of Eq. (85) has two extremum points: a minimum at $\mathcal{V} = 1/3$ (outside the physical domain) and a maximum at $\mathcal{V} = 1$, where $\mathcal{T} = 1$. Accordingly, Eq. (85) is never satisfied for $\mathcal{T} > 1$, which implies no extremum point for related isothermals, as expected. The contrary holds for $\mathcal{T} < 1$, where it can be seen that the third-degree equation associated to Eq. (83) has three real solutions, related to extremum points. One lies outside the physical domain, which implies $\mathcal{V} \leq 1/3$. The remaining two are obtained as the intersections between the curve, $y = f(\mathcal{V})$, expressed by Eq. (85), and the straight line, $y = \mathcal{T}$, keeping in mind that $f(1/3) = 0$, $f(1) = 1$, and $\lim_{\mathcal{V} \rightarrow +\infty} f(\mathcal{V}) = 0$.

The third-degree equation associated to Eq. (83), may be ordered as:

$$\mathcal{V}^3 - 9a\mathcal{V}^2 + 6a\mathcal{V} - a = 0 ; \quad (86a)$$

$$a = \frac{1}{4\mathcal{T}} ; \quad (86b)$$

where, with regard to the standard formulation (e.g., Spiegel, 1968, Chap. 9):

$$x^3 + a_1x^2 + a_2x + a_3 = 0 ; \quad (87)$$

the discriminants of Eq. (86a) are:

$$Q = \frac{3a_2 - a_1^2}{9} = a(2 - 9a) ; \quad (88)$$

$$R = \frac{9a_1a_2 - 27a_3 - 2a_1^3}{54} = \frac{a(1 - 18a + 54a^2)}{2} ; \quad (89)$$

$$D = Q^3 + R^2 = \frac{a^2(1 - 4a)}{4} ; \quad (90)$$

where $D = 0$ in the special case of the critical isothermal ($\mathcal{T} = 1, a = 1/4$), $D < 0$ for $\mathcal{T} < 1$, and $D > 0$ for $\mathcal{T} > 1$. Accordingly, three (at least two coincident) real solutions exist if $D = 0$, three different real solutions if

$D < 0$, one real and two complex conjugate if $D > 0$. A real solution, \mathcal{V}_0 , always lies outside the physical domain.

The three real solutions ($D \leq 0$) may be expressed as (e.g., Spiegel, 1968, Chap. 9):

$$\mathcal{V}_1 = 2\sqrt{-Q} \cos\left(\pi + \frac{\theta}{3} + \frac{0\pi}{3}\right) - \frac{1}{3}a_1 ; \quad (91a)$$

$$\mathcal{V}_2 = 2\sqrt{-Q} \cos\left(\pi + \frac{\theta}{3} + \frac{2\pi}{3}\right) - \frac{1}{3}a_1 ; \quad (91b)$$

$$\mathcal{V}_3 = 2\sqrt{-Q} \cos\left(\pi + \frac{\theta}{3} + \frac{4\pi}{3}\right) - \frac{1}{3}a_1 ; \quad (91c)$$

$$\theta = \arctan\left(\frac{\sqrt{-D}}{R}\right) ; \quad (91d)$$

where $a_1 = -9a$ and, in the special case of critical isothermal, $a = 1/4$, $Q = -1/16$, $R = -1/64$, $D = 0$, which implies $\mathcal{V}_0 = \min(\mathcal{V}_1, \mathcal{V}_2, \mathcal{V}_3)$, $\mathcal{V}_A = \mathcal{V}_B = \mathcal{V}_C = \mathcal{V}_D = \mathcal{V}_E = \max(\mathcal{V}_1, \mathcal{V}_2, \mathcal{V}_3)$. A null factor appears in Eq. (91a) to save aesthetics. In the special case, $\mathcal{T} \rightarrow 0$, Eq. (86a) reduces to a second-degree equation whose solutions are $\mathcal{V}_{01} = \mathcal{V}_{02} = 1/3$, while the related function is otherwise divergent as $a \rightarrow +\infty$. In general, the extremum points of VDW isothermals ($\mathcal{T} \leq 1$) occur at $\mathcal{V} = \mathcal{V}_B$ (minimum) and $\mathcal{V} = \mathcal{V}_D$ (maximum), $\mathcal{V}_B \leq \mathcal{V}_D$. As $\mathcal{T} \rightarrow 0$, $\mathcal{V}_B \rightarrow 1/3$, $\mathcal{V}_D \rightarrow +\infty$, where, in all cases, $1/3 < \mathcal{V}_B \leq 1 \leq \mathcal{V}_D$.

B Intersections between real and VDW isothermals of equal temperature

With regard to selected real and VDW isothermals of equal temperature, three distinct intersections occur in presence of saturated vapour i.e. below the critical temperature, which are coincident at the critical temperature. Vapour pressure maintains constant in presence of liquid phase i.e. $\mathcal{V}_A \leq \mathcal{V} \leq \mathcal{V}_E$, where an infinitesimal vapour and liquid mass fraction characterizes the extreme reduced volume values, \mathcal{V}_A and \mathcal{V}_E , respectively. In presence of a sole phase, liquid ($\mathcal{V} < \mathcal{V}_A$) or gas ($\mathcal{V} > \mathcal{V}_E$), related real and VDW isothermal branches coincide.

The intersections between real and VDW isothermals of equal temperature (within the range where they are different) can be determined as intersections between horizontal lines and VDW isothermals on the Clapeyron reduced plane. Two intersections necessarily occur at $(\mathcal{V}_A, \mathcal{p}_A)$ and $(\mathcal{V}_E, \mathcal{p}_E)$.

The third one, $(\mathcal{V}_C, \mathcal{p}_C)$, necessarily lies between the other two where, in addition, $\mathcal{p}_A = \mathcal{p}_C = \mathcal{p}_E$. The coordinates of the extremum points, $(\mathcal{V}_B, \mathcal{p}_B)$, minimum, and $(\mathcal{V}_D, \mathcal{p}_D)$, maximum, must necessarily satisfy the following inequalities: $\mathcal{V}_A \leq \mathcal{V}_B \leq \mathcal{V}_C$; $\mathcal{V}_C \leq \mathcal{V}_D \leq \mathcal{V}_E$; $\mathcal{p}_B \leq \mathcal{p}_C \leq \mathcal{p}_D$. It can be seen that regions, ABC, CDE, bounded by real and VDW isothermals with equal temperature, have equal areas (e.g., LL67, Chap. VIII, §85), which yields the following relation (e.g., C10):

$$\mathcal{p}_C = \frac{8}{3} \frac{\mathcal{T}}{\mathcal{V}_E - \mathcal{V}_A} \ln \frac{3\mathcal{V}_E - 1}{3\mathcal{V}_A - 1} - \frac{3}{\mathcal{V}_A \mathcal{V}_E} ; \quad (92)$$

where, for a selected isothermal, the unknowns are $\mathcal{p}_C = \mathcal{p}_A = \mathcal{p}_E$, \mathcal{V}_A , and \mathcal{V}_E .

The reduced volumes, \mathcal{V}_A , \mathcal{V}_C , \mathcal{V}_E , see Fig. 3, may be considered as intersections between a VDW isothermal ($\mathcal{T} < 1$) and a horizontal straight line, $\mathcal{p} = \mathcal{p}_C$, on the Clapeyron reduced plane. In other words, \mathcal{V}_A , \mathcal{V}_C , \mathcal{V}_E , are the real solutions of the third-degree equation:

$$\mathcal{V}^3 - \left(\frac{1}{3} + \frac{8}{3} \frac{\mathcal{T}}{\mathcal{p}_C} \right) \mathcal{V}^2 + \frac{3}{\mathcal{p}_C} \mathcal{V} - \frac{1}{\mathcal{p}_C} = 0 ; \quad (93)$$

which has been deduced from Eq. (82), particularized to $\mathcal{p} = \mathcal{p}_C$. Related solutions may be calculated using Eqs. (91). The last unknown, \mathcal{p}_C , is determined from Eq. (92).

An inspection of Fig. 3 shows that the points, A and E, are located on the left of the minimum, B, and on the right of the maximum, D, respectively. Keeping in mind the above results, the following inequality holds: $\mathcal{V}_A \leq \mathcal{V}_B \leq 1 \leq \mathcal{V}_D \leq \mathcal{V}_E$, which implies further investigation on the special case, $\mathcal{V}_C = 1$. The particularization of VDW equation of state, Eq. (82), to the point, C = C₁, assuming $\mathcal{V}_{C_1} = 1$, yields:

$$\mathcal{T} = \frac{\mathcal{p}_{C_1} + 3}{4} ; \quad (94)$$

and Eq. (93) reduces to:

$$\mathcal{V}^3 - (1 + 2b)\mathcal{V}^2 + 3b\mathcal{V} - b = 0 ; \quad (95a)$$

$$b = \frac{1}{\mathcal{p}_{C_1}} ; \quad (95b)$$

with regard to the generic third-degree equation, Eq. (87), the three solutions, x_1 , x_2 , x_3 , satisfy the relations (e.g., Spiegel, 1968, Chap. 9):

$$x_1 + x_2 + x_3 = -a_1 ; \quad (96a)$$

$$x_1x_2 + x_2x_3 + x_3x_1 = a_2 ; \quad (96b)$$

$$x_1x_2x_3 = -a_3 ; \quad (96c)$$

where, in the case under discussion:

$$a_1 = -1 - 2b \ ; \quad a_2 = 3b \ ; \quad a_3 = -b \ ; \quad (97a)$$

$$x_1 = \mathcal{V}_A \ ; \quad x_2 = \mathcal{V}_{C_1} = 1 \ ; \quad x_3 = \mathcal{V}_E \ ; \quad (97b)$$

and the substitution of Eqs. (97) into two among (96) yields:

$$\mathcal{V}_A = b - \sqrt{b^2 - b} \ ; \quad (98a)$$

$$\mathcal{V}_E = b + \sqrt{b^2 - b} \ ; \quad (98b)$$

finally, the combination of Eqs. (94), (95b), and (98) produces:

$$\mathcal{V}_A = \frac{1 - 2\sqrt{1 - \mathcal{T}}}{4\mathcal{T} - 3} \ ; \quad \mathcal{T} \leq 1 \ ; \quad (99a)$$

$$\mathcal{V}_E = \frac{1 + 2\sqrt{1 - \mathcal{T}}}{4\mathcal{T} - 3} \ ; \quad \mathcal{T} \leq 1 \ ; \ ; \quad (99b)$$

which, together with $\mathcal{V}_{C_1} = 1$, are the abscissae of the intersection points between a selected VDW isothermal on the Clapeyron reduced plane and the straight line, $\mathcal{p} = \mathcal{p}_{C_1}$, in the special case under discussion.

The substitution of Eqs. (99) into (92), the last related to $\mathcal{p} = \mathcal{p}_{C_1}$ via Eq. (94), yields:

$$\frac{\mathcal{T}}{\sqrt{1 - \mathcal{T}}} \ln \frac{3 - 2\mathcal{T} + 3\sqrt{1 - \mathcal{T}}}{3 - 2\mathcal{T} - 3\sqrt{1 - \mathcal{T}}} = 6 \ ; \quad (100)$$

which, keeping in mind the limit:

$$\lim_{x \rightarrow 0} \left[\frac{1}{x} \ln \frac{1 + x}{1 - x} \right] = 2 \ ; \quad (101)$$

holds only for the critical isothermal, $\mathcal{T} = 1$. Accordingly, the abscissa of the intersection point, \mathbf{C} , between a selected VDW isothermal and related real isothermal, see Fig. 3, cannot occur at $\mathcal{V}_C = 1$ unless the critical isothermal is considered. Then the third-degree equation, Eq. (93), must be solved in the general case ($\mathcal{V}_C \neq 1$) by use of Eqs. (91).

C The limit of zero absolute temperature

Ideal gas equation of state, expressed by Eq. (1), in the limit of zero absolute temperature, $T = 0$ K, implies (i) pressure attains any value, $p > 0$, provided

$V \rightarrow 0$, and (ii) volume attains any value, $V > 0$, provided $p \rightarrow 0$. Accordingly, related ideal isothermal on the Clapeyron plane, (OVp) , tends to positive coordinate semiaxes. The same holds for reduced variables on the Clapeyron reduced plane, $(O\mathcal{V}\mathcal{p})$.

VDW equation of state, expressed by Eq. (2), in the limit of zero absolute temperature, $T = 0\text{ K}$, implies (i) pressure attains any value, $p > -A/B^2$, provided $V \rightarrow NB$, and (ii) volume attains any value, $V > NB$, provided $p \rightarrow -A/B^2$; where $NB = V_c/3$; $A/B^2 = 27p_c$; via Eqs. (3); (5); respectively. Accordingly, related VDW isothermal on the Clapeyron plane, (OVp) , tends to subdomains, $V > V_c/3$; $p > -27p_c$; or, in reduced variables, $\mathcal{V} > 1/3$; $\mathcal{p} > -27$; respectively.

With regard to VDW isothermal in the limit of absolute zero reduced temperature, $\mathcal{T} \rightarrow 0$, extremum points occur at $\mathcal{V}_B \rightarrow 1/3$ (minimum) and $\mathcal{V}_D \rightarrow +\infty$ (maximum), as inferred in Appendix A and, in addition, $\mathcal{p}_B \rightarrow -27$ (minimum) and $\mathcal{p}_D \rightarrow 0$ (maximum), according to above considerations. In summary, $B \rightarrow B_0 \equiv (1/3, -27)$ and $D \rightarrow D_0 \equiv (+\infty, 0)$.

The real isothermal ($\mathcal{V}_A \leq \mathcal{V} \leq \mathcal{V}_E$) in the limit of absolute zero reduced temperature, $\mathcal{T} \rightarrow 0$, can be determined via Eq. (92) keeping in mind $\mathcal{V}_B \geq \mathcal{V}_A$ and $\mathcal{V}_D \leq \mathcal{V}_E$. The result is $\mathcal{p}_C \rightarrow 0$.

In general, intersections between VDW isothermals and horizontal lines, $\mathcal{p} = \mathcal{p}_C$, on the Clapeyron reduced plane, $(O\mathcal{V}\mathcal{p})$, are solution of a third-degree equation expressed by Eq. (93) which, in the special case of the horizontal axis, $\mathcal{p}_C = 0$, reduces to a second-degree equation, as:

$$\frac{8}{3}\mathcal{T}\mathcal{V}^2 + 3\mathcal{V} - 1 = 0 \quad ; \quad (102)$$

and related solutions read:

$$\mathcal{V} = \frac{9 \mp \sqrt{81 - 96\mathcal{T}}}{16\mathcal{T}} \quad ; \quad (103)$$

where real solutions imply $\mathcal{T} \leq 81/96 = 27/32$ and the special case, $\mathcal{T} = 27/32$, yields a VDW isothermal which is tangent to the horizontal axis on $(\mathcal{V}_B, 0)$. If, in particular, $\mathcal{p}_C = 0$ and $\mathcal{T} \rightarrow 0$, Eq. (93) reduces to a first-degree equation, as:

$$3\mathcal{V} - 1 = 0 \quad ; \quad (104)$$

and related solution reads $\mathcal{V} = 1/3$, as expected.

To get further insight, let a variable, x , be defined as:

$$81 - 96\mathcal{T} = x^2 \quad ; \quad \mathcal{T} = \frac{81 - x^2}{96} \quad ; \quad 0 \leq x < 9 \quad ; \quad (105)$$

where the limit of zero absolute reduced temperature, $\mathcal{T} \rightarrow 0^+$, relates to $x \rightarrow 9^-$. The substitution of Eq. (105) into (103) yields:

$$\mathcal{V} = \frac{9 \mp x}{16(81 - x^2)/96} = \frac{96}{16} \frac{9 \mp x}{(9 + x)(9 - x)} = \frac{6}{9 \pm x} ; \quad (106)$$

with regard to VDW isothermals, $\mathcal{T} = (81 - x^2)/96$. In the limit of zero absolute reduced temperature, $x \rightarrow 9^-$, the above solutions read $\mathcal{V} \rightarrow 6/18 = 1/3$ and $\mathcal{V} \rightarrow +\infty$, as expected.

VDW isothermals are plotted in Fig. 12 for integer x , $0 \leq x \leq 8$, where values related to negative pressure or sufficiently small volume are not shown for sake of clarity. An inspection of Fig. 12 shows regions, ABC, CDE, bounded by real and VDW reduced isothermals (e.g., Fig. 3), exhibit equal areas (e.g., LL67, Chap. VII, §85) which increase as reduced temperature decreases and tend to infinite as $\mathcal{T} \rightarrow 0$.

More specifically, the trend is described by the following relations:

$$\begin{aligned} \mathcal{V}_A &\rightarrow \frac{1}{3} ; \mathcal{V}_B \rightarrow \frac{1}{3} ; \mathcal{V}_C \rightarrow +\infty ; \mathcal{V}_D \rightarrow +\infty ; \mathcal{V}_E \rightarrow +\infty ; \mathcal{T} \rightarrow 0 ; \\ \phi_A &\rightarrow 0 ; \phi_B \rightarrow -27 ; \phi_C \rightarrow 0 ; \phi_D \rightarrow 0 ; \phi_E \rightarrow 0 ; \mathcal{T} \rightarrow 0 ; \end{aligned}$$

according to above considerations where, in general (e.g., Fig. 3):

$$\begin{aligned} \mathcal{V}_A &\leq \mathcal{V}_B \leq \mathcal{V}_C \leq \mathcal{V}_D \leq \mathcal{V}_E ; \quad \mathcal{T} \leq 1 ; \\ \phi_B &\leq \phi_A = \phi_C = \phi_E \leq \phi_D ; \quad \mathcal{T} \leq 1 ; \end{aligned}$$

according to the results of Appendix B.

The limit of zero absolute reduced temperature, $\mathcal{T} \rightarrow 0$, implies (i) region ABC tends to a rectangular triangle of catheti, $\overline{AB} = \phi_A - \phi_B = 27$ and $\overline{AC} = \mathcal{V}_C - \mathcal{V}_A \rightarrow +\infty$; (ii) region CDE tends to a triangle of height, $\phi_D - \phi_C = \phi_D - \phi_E \rightarrow 0$, and basis, $\mathcal{V}_E - \mathcal{V}_C \rightarrow +\infty$; and (iii) regions ABC and CDE exhibit infinite area of same order, where their ratio equals unity.

D Fractional macroisothermals

In considering whether fractional macroisothermals, $Y_T = (T_P/T_G) = (\overline{m}_P/\overline{m}_G)$ ($\phi/m = \text{const}$ via Eqs. (37) and (40), hence $\phi/m = \text{const}$, are a viable alternative with respect to fractional isoenergetics, $X_T = \phi = \text{const}$ via Eqs. (39) and (42), for determining isoenergetics or macroisothermals, attention shall be restricted in finding a counterexample.

With regard to UU macrogases, the following relation holds (C10):

$$\frac{\phi}{m} = \begin{cases} \frac{(2m+5)y^2-3}{2(y^3+m)} ; & 1 \leq y < +\infty ; \\ \frac{2(y^3+m)}{(2+5m)y-3my^3} ; & 0 < y \leq 1 ; \end{cases} \quad (107)$$

where $y = 1$ implies $\phi/m = 1$, independent of m , according to Eq. (43). Related fractional macroisothermal reads:

$$(2m + 5)y^2 - 3 = 2(y^3 + m) \ ; \quad 1 \leq y < +\infty \ ; \quad (108a)$$

$$2(y^3 + m) = (2 + 5m)y - 3my^3 \ ; \quad 0 < y \leq 1 \ ; \quad (108b)$$

which, after some algebra, may be cast under the form:

$$m = \begin{cases} \frac{2y^3 - 5y^2 + 3}{2(y^2 - 1)} = \frac{2y^2 - 3y - 3}{2(y + 1)} \ ; \ 1 \leq y < +\infty \ ; \\ \frac{2y(1 - y^2)}{3y^3 - 5y + 2} = \frac{-2y(y + 1)}{3y^2 + 3y - 2} \ ; \ 0 < y \leq 1 \ ; \end{cases} \quad (109)$$

and the function, $m = m(y)$, can be studied.

Special values are the following:

$$m(0) = 0 \ ; \quad m(1) = -1 \ ; \quad \lim_{y \rightarrow +\infty} m(y) = \lim_{y \rightarrow +\infty} y = +\infty \ ; \quad (110)$$

where, in addition to the origin, zeroes of $m(y)$ are solutions of the second-degree equation, $2y^2 - 3y - 3 = 0$, hence $y = (3 \mp \sqrt{9 + 24})/4$, and the zero within the domain, $y \geq 1$, reads:

$$m\left(\frac{3 + \sqrt{33}}{4}\right) = 0 \ . \quad (111)$$

On the other hand, vertical asymptotes relate to solutions of the second-degree equation, $3y^2 + 3y - 2 = 0$, hence $y = (-3 \mp \sqrt{9 + 24})/6$, and the vertical asymptote within the domain, $0 \leq y \leq 1$, reads:

$$\lim_{y \rightarrow y_0^\mp} m(y) = \pm\infty \ ; \quad y_0 = \frac{-3 + \sqrt{33}}{6} \ . \quad (112)$$

The above results define the sign of $m(y)$ all over the domain, as:

$$0 \leq y \leq \frac{\sqrt{33} - 3}{6} \ ; \quad m(y) \geq 0 \ ; \quad (113a)$$

$$\frac{\sqrt{33} - 3}{6} \leq y \leq \frac{\sqrt{33} + 3}{4} \ ; \quad m(y) \leq 0 \ ; \quad (113b)$$

$$\frac{\sqrt{33} + 3}{4} \leq y < +\infty \ ; \quad m(y) \geq 0 \ ; \quad (113c)$$

accordingly, the mass ratio, m , can assume both signs.

But $m \geq 0$ by definition, which implies homodirection axis ratios, y , within the range defined by Eq. (113b), cannot occur along the fractional macroisothermal, $\phi/m = 1$. For this reason, it would be better dealing with fractional isoenergetics, where the above mentioned inconvenient does not take place.

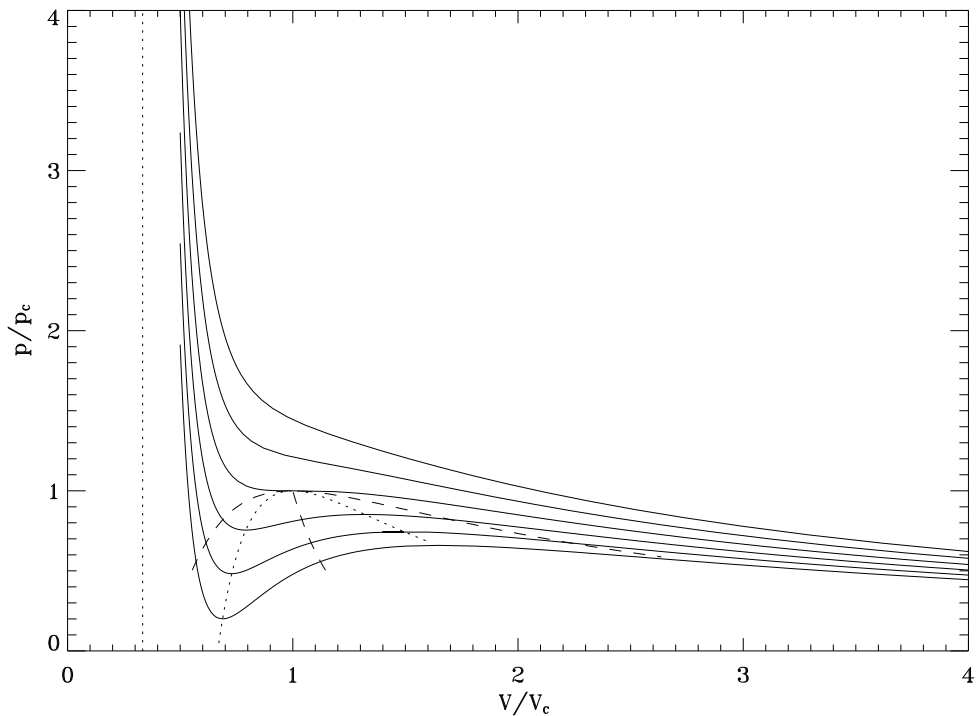


Figure 2: Same as in Fig. 1 (right panel), where the occurrence (within the area bounded by the bell-shaped dashed curve) of saturated vapour is considered. Above the critical isothermal ($T/T_c = 1$) the trend is similar with respect to ideal gases. Below the critical isothermal and on the right of the bell-shaped dashed curve, gas still behaves as an ideal gas. Below the critical isothermal and on the left of the bell-shaped dashed curve, liquid shows little change in volume as pressure rises. Within the area bounded by the bell-shaped dashed curve, liquid phase is in equilibrium with saturated vapour phase. A diminished volume implies smaller saturated vapour fraction and larger liquid fraction at constant pressure, and vice versa. VDW equation of state is no longer valid in this region. The dashed curve (including the central branch) is the locus of intersections between VDW and real isotherms, the latter being related to constant pressure where liquid and vapour phases coexist. Ending points are $(1/3, 0)$, left; $(+\infty, 0)$, middle; $(+\infty, 0)$, right. The dotted curve is the locus of VDW isothermal extremum points. Ending points are $(1/3, -27)$, left; $(+\infty, 0)$, right.

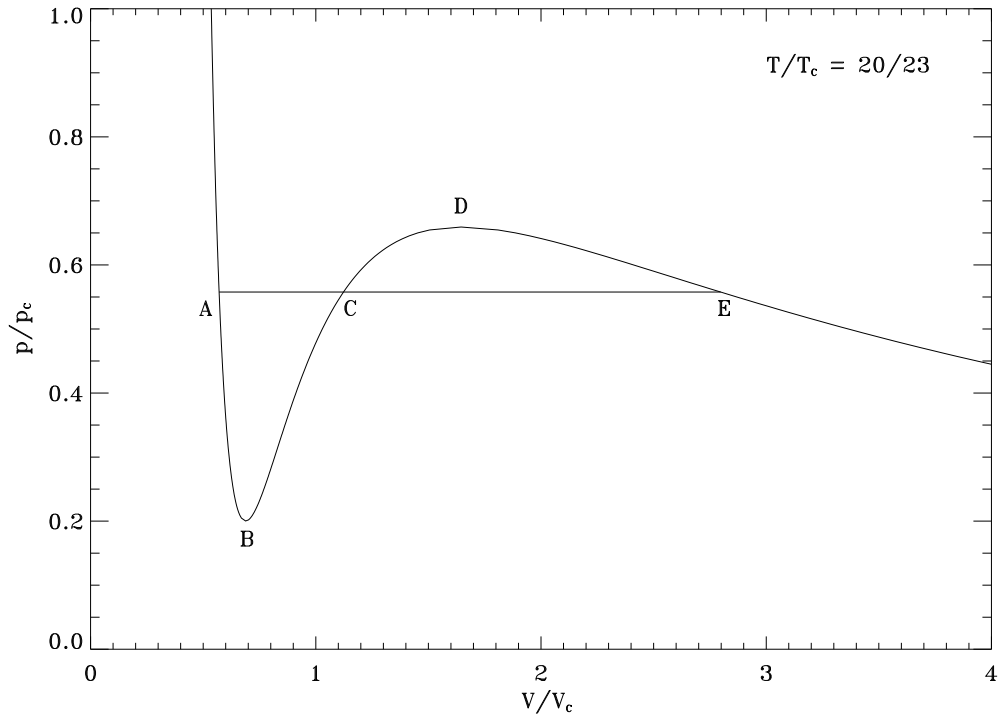


Figure 3: VDW and real isothermals with equal temperature, $T/T_c = 20/23$. The two curves coincide within the range, $V \leq V_A$ and $V \geq V_E$. VDW isotherm exhibits two extremum points: minimum, **B**, and maximum, **D**, while real isotherm is flat within the range, $V_A \leq V \leq V_E$. Configurations related to VDW isotherm within the range, $V_A \leq V \leq V_B$ (due to tension forces acting on particles, yielding superheated liquid), and $V_D \leq V \leq V_E$ (due to the occurrence of undercooled vapour), may be obtained under special conditions, while configurations within the range, $V_B \leq V \leq V_D$, are always unstable. Volumes, V_A and V_E , correspond to maximum value in presence of sole liquid phase and minimum value in presence of sole vapour phase, respectively. Regions, **ABC** and **CDE**, exhibit equal area.

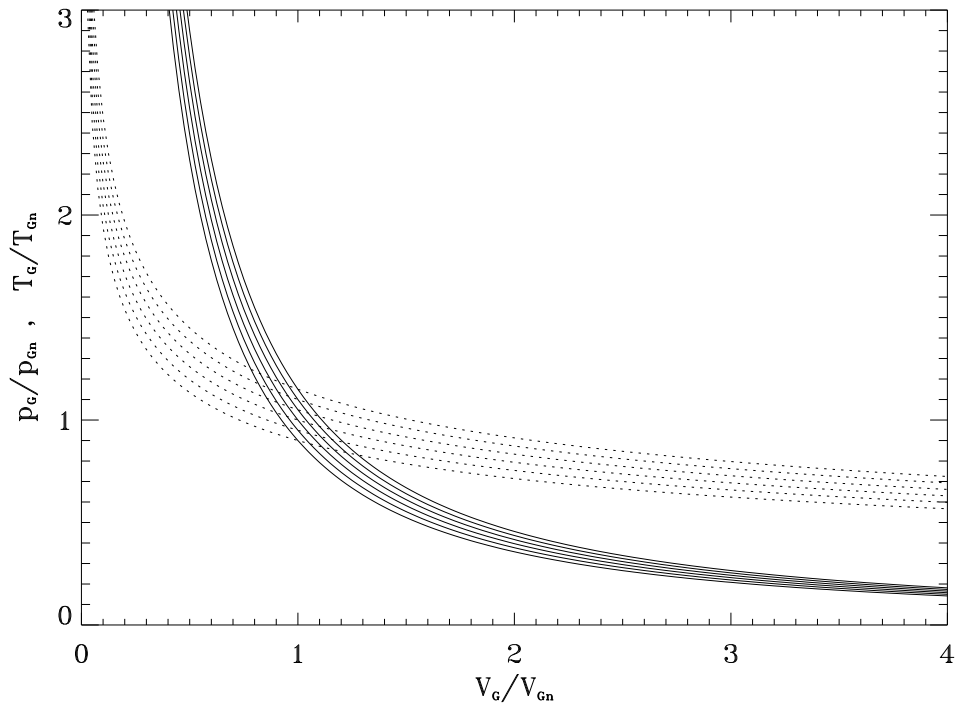


Figure 4: Reduced macropressure, p_G , and reduced macrotemperature, T_G , vs reduced volume, V_G , for $\kappa = 0.90, 0.95, 1.00, 1.05, 1.10, 1.15$, from bottom to top, where $\kappa = M_G^2$ for reduced macropressure (full curves) and $\kappa = M_G \chi_c$ for reduced macrotemperature (dotted curves).

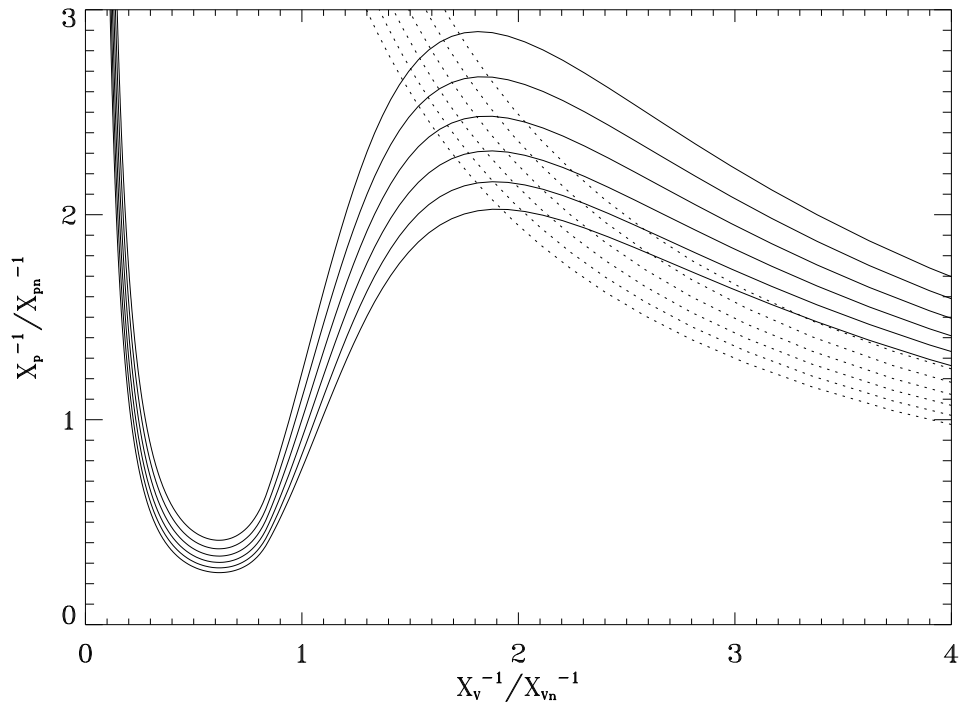


Figure 5: Fractional isoenergetics related to UU macrogases for $X_T^{-1} = 20/23, 20/22, 20/21, 20/20, 20/19, 20/18$, from bottom to top. The contribution from the term, X_T^{-1}/X_V^{-1} , is shown by dotted curves. Normalization values are $(X_{Vn}, X_{pn}, X_{Tn}) = (0.8425, 53.15545, 10)$.

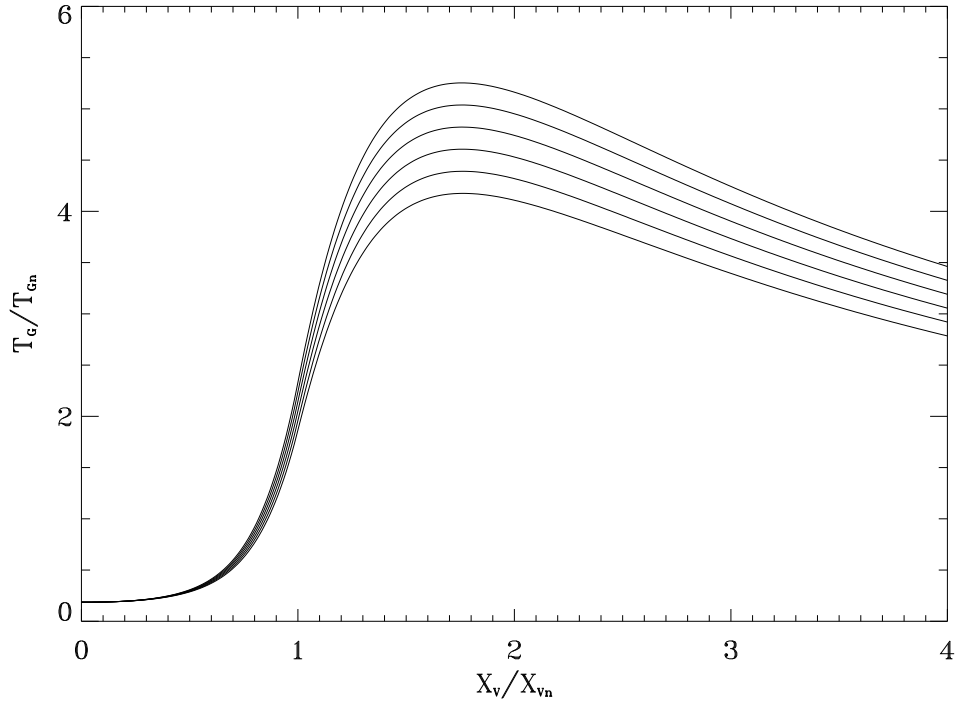


Figure 6: Reduced macrotemperature, T_G , vs reduced variable, X_V , related to UU macrogases for $M_G^{-1} \Psi_G^{1/3} = 1$ and $X_T^{-1} = 20/23, 20/22, 20/21, 20/20, 20/19, 20/18$, from bottom to top. A similar trend is exhibited for critical fractional isoenergetic, $X_T^{-1} = 1$, and $M_G^{-1} \Psi_G^{1/3} = 20/23, 20/22, 20/21, 20/20, 20/19, 20/18$, from bottom to top.

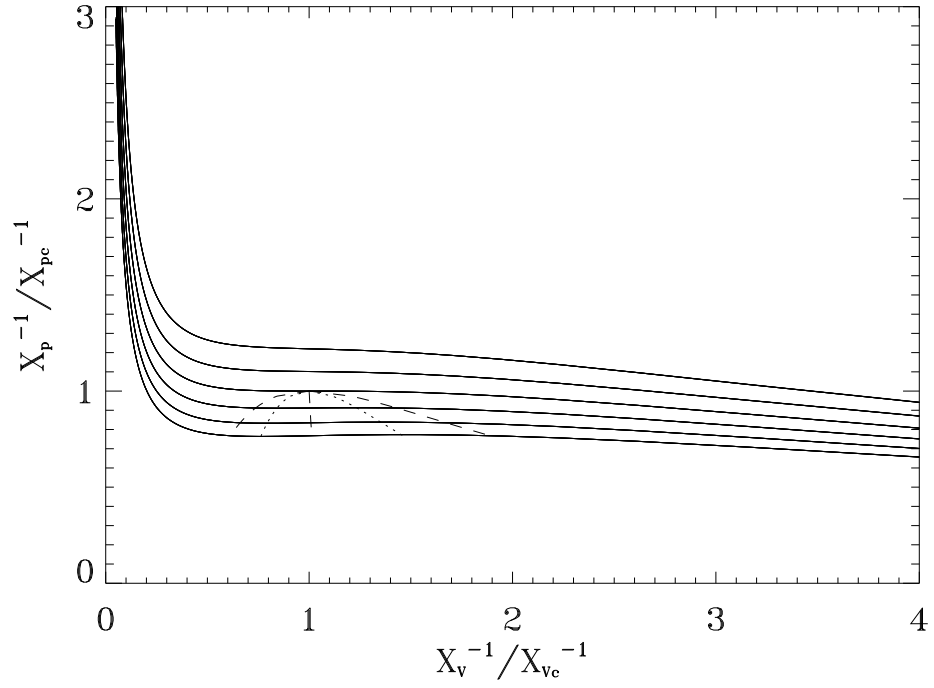


Figure 7: Fractional isoenergetics related to HH macrogases for $\mathcal{X}_T^{-1} = 20/23, 20/22, 20/21, 20/20, 20/19, 20/18$, from bottom to top, where cases, $\Xi_G/\Xi_P = 0.25, 0.50, 1.00, 2.00, 4.00$, are superimposed. The dashed curve (including central branch) is the locus of intersections between HH fractional isoenergetics and horizontal lines yielding regions of equal area. The dotted curve is the locus of HH fractional isoenergetic extremum points. Plotting \mathcal{X}_p^{-1} vs \mathcal{X}_v^{-1} yields fractional isoenergetics similar to VDW isothermals shown in Fig. 2, where extremum points are lying below the critical point.

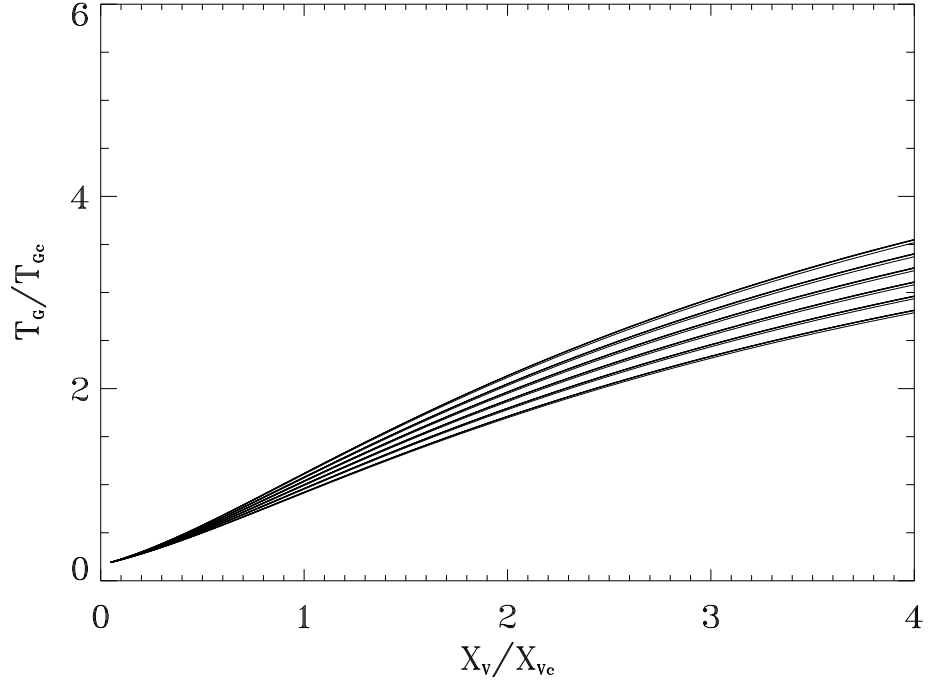


Figure 8: Fractional macrotemperature, T_G , vs reduced variable, X_V , related to HH macrogases for $M_G^{-1} V_G^{1/3} = 1$ and $X_T^{-1} = 20/23, 20/22, 20/21, 20/20, 20/19, 20/18$, from bottom to top, where cases, $\Xi_G/\Xi_P = 0.25, 0.50, 1.00, 2.00, 4.00$, are superimposed. A similar trend is exhibited for critical fractional isoenergetic, $X_T^{-1} = 1$, and $M_G^{-1} V_G^{1/3} = 20/23, 20/22, 20/21, 20/20, 20/19, 20/18$, from bottom to top.

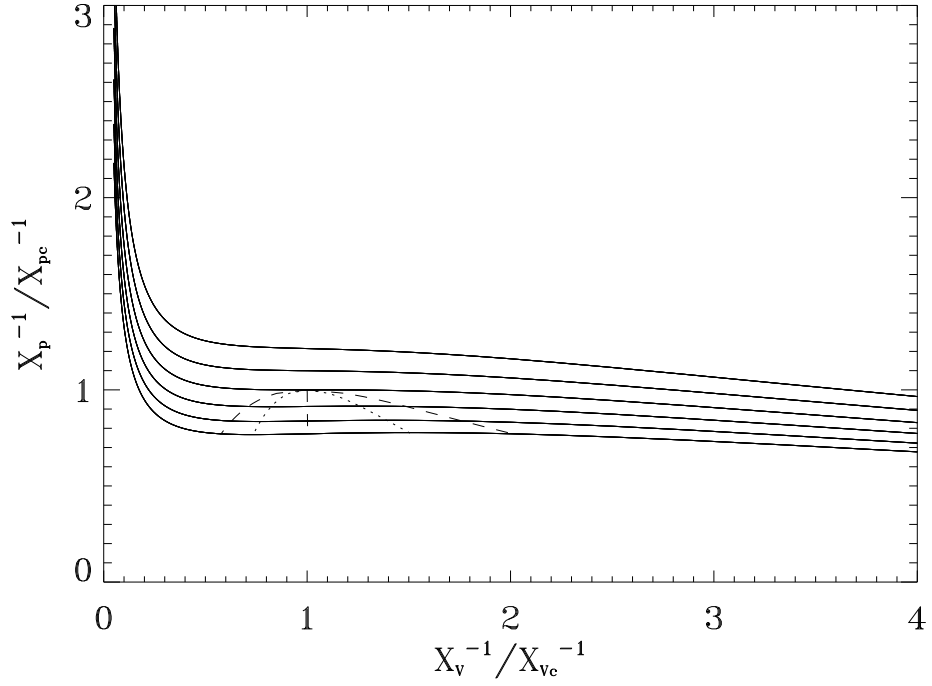


Figure 9: Fractional isoenergetics related to HN/NH macrogases for $X_T^{-1} = 20/23, 20/22, 20/21, 20/20, 20/19, 20/18$, from bottom to top, where cases, $\Xi_G/\Xi_P = 0.25, 0.50, 1.00, 2.00, 4.00$, are superimposed. The dashed curve (including central branch) is the locus of intersections between HN/NH fractional isoenergetics and horizontal lines yielding regions of equal area. The dotted curve is the locus of HN/NH fractional isoenergetic extremum points. Plotting X_p^{-1} vs X_v^{-1} yields fractional isoenergetics similar to VDW isothermals shown in Fig. 2, where extremum points are lying below the critical point.

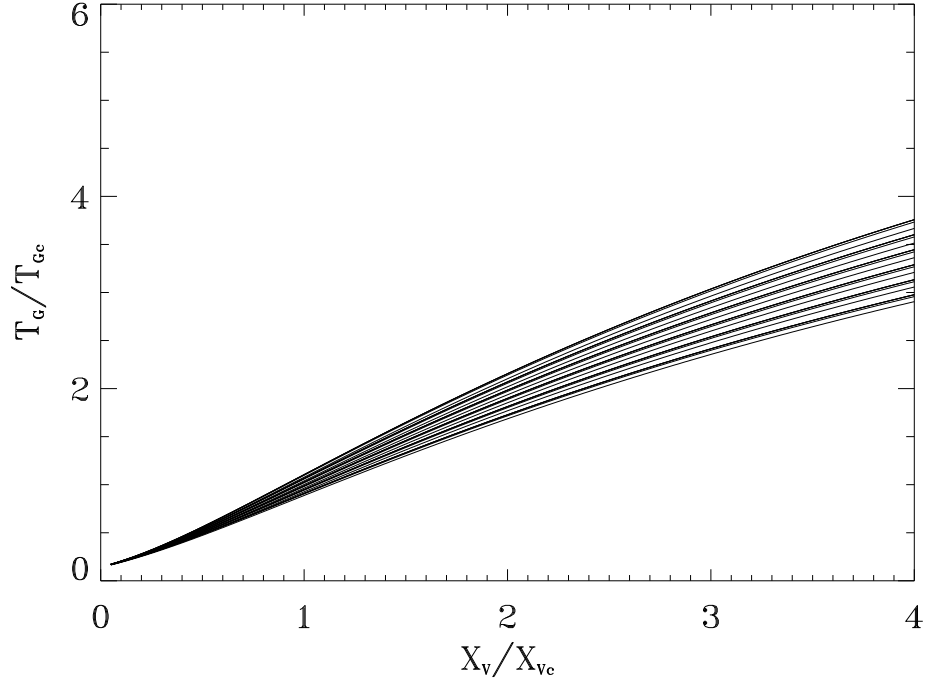


Figure 10: Reduced macrotemperature, T_G , vs reduced variable, X_V , related to HN/NH macrogases for $M_G^{-1} \Psi_G^{1/3} = 1$ and $X_T^{-1} = 20/23, 20/22, 20/21, 20/20, 20/19, 20/18$, from bottom to top, where cases, $\Xi_G/\Xi_P = 0.25, 0.50, 1.00, 2.00, 4.00$, are superimposed. A similar trend is exhibited for critical fractional isoenergetic, $X_T = 1$, and $M_G^{-1} \Psi_G^{1/3} = 20/23, 20/22, 20/21, 20/20, 20/19, 20/18$, from bottom to top.

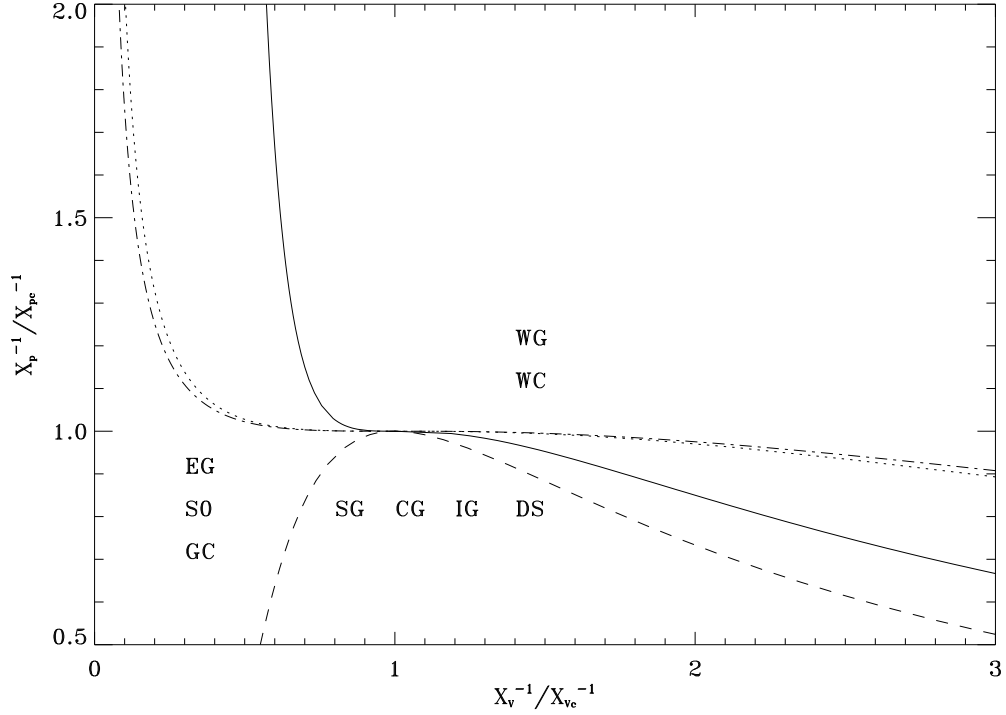


Figure 11: Comparison between VDW critical isothermal (full), HH critical fractional isoenergetic (dotted), and HN/NH critical fractional isoenergetic (dot-dashed). With regard to ordinary fluids, vapour and liquid phase co-exist within the bell-shaped region bounded by the dashed curve and, in addition, $X_V^{-1} = V$, $X_P^{-1} = p$. More extended (along the horizontal direction) bell-shaped regions are expected for both HH and HN/NH fractional isoenergetics. The critical point, by definition, reads $(X_{V_c}, X_{P_c}, X_{T_c}) \equiv (1, 1, 1)$. Different letters denote expected location of different astrophysical systems. Caption: EG - elliptical galaxies; S0 - lenticular galaxies; SG - spiral galaxies including barred; IG - irregular galaxies; DS - dwarf spheroidal galaxies; GC - globular clusters; CG - galaxy clusters; WC - wholly gaseous clouds where stars never formed; WG - (hypothetical) wholly gaseous galaxies where stars never formed.

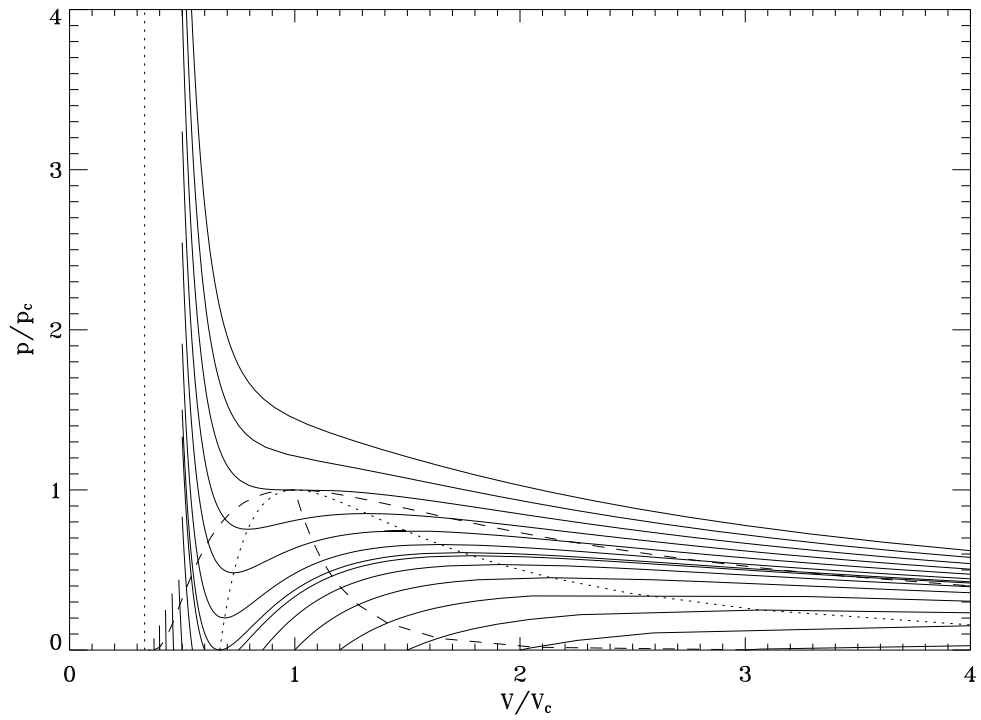


Figure 12: VDW isothermals, $\mathcal{T} = (81 - x^2)/96$, plotted for integer x , $0 \leq x \leq 8$, from top to bottom where the first is tangent to the horizontal axis and the last lies outside the box. The region of negative pressure or sufficiently small volume is not shown for sake of clarity. In the limit of zero absolute reduced temperature, $\mathcal{T} \rightarrow 0^+$, $x \rightarrow 9^-$, VDW isothermal reads $\phi > -27$; $\Psi \rightarrow 1/3$; and $\phi \rightarrow -27$; $\Psi > 1/3$. Other curves and captions as in Fig. 2.